



PPRIME INSTITUTE

INTERNSHIP REPORT

PFE-MASTER

**FUNDAMENTAL STUDY OF PLASMA
JET-LIQUID INTERACTION BY FREE
SURFACE TOPOGRAPHY**

01/04/2021 - 01/10/2021

Author :

M. João Vítor DIAS HONORATO DE OLIVEIRA

Chasseneuil du Poitou

September 7, 2021

Internship Supervisor :

M. Thomas ORRIÈRE

M. Guillaume GOMIT

Contents

1	INTRODUCTION	2
2	BIBLIOGRAPHY	3
3	METHOD	7
3.1	FREE-SURFACE SYNTHETIC SCHLIEREN	8
3.2	SHADOWGRAPH	11
3.3	EXPERIMENTAL SETUP	12
3.4	PARAMETERS AND TREATMENTS	15
3.5	VALIDATION	16
3.6	LIMITATIONS	19
4	MEASUREMENT WITHOUT PLASMA	20
4.1	NEGATIVE VERSUS POSITIVE DEFORMATION	20
4.2	NEGATIVE AND POSITIVE VOLTAGE STUDY	22
4.3	GAS FLOW RATES	24
4.4	GAS FLOW RATES WITH NEGATIVE ELECTRIC FIELD	25
4.5	GAS FLOW RATES WITH POSITIVE ELECTRIC FIELD	26
5	MEASUREMENT WITH PLASMA	28
5.1	NEGATIVE DISCHARGE	29
5.1.1	ELECTRICAL CURRENT	31
5.1.1.1	CURRENT VARIATION FOR 5SCCM	32
5.1.1.2	CURRENT VARIATION FOR 10SCCM AND 15SCCM	33
5.1.1.3	CURRENT VARIATION FOR 25SCCM	35
5.1.2	GAS FLOW RATES	35
5.1.2.1	ARGON FLOW CHANGES FOR 1,5mA	36
5.1.2.2	ARGON FLOW CHANGES FOR 3mA	38
5.1.2.3	ARGON FLOW CHANGES FOR 4,5mA	39
5.2	POSITIVE DISCHARGE	40
6	CONCLUSION	43
7	APPENDIX	48

1 INTRODUCTION

This research has been made in the Pprime institute, an institute specialized in the fields of Physics and Engineering Sciences. It is a UPR CNRS linked with the University of Poitiers and ISAE-ENSMA. More specifically, the internship took place in the Electrofluidynamic team in the field of Plasma Jet.

The plasma sector has a very wide range of applications. It can be used in as many applications as imagined, from cutting thick metal sheets to sterilisation of objects. To each application a different kind of plasma is more suitable. To obtain those different configurations of plasma, normally a high voltage system is needed but also different means, electrodes, power or method can be chosen.

Here, it was used a low-power DC atmospheric pressure micro plasma jet, with an inert gas. The plasma jet was an ignited arc in an argon jet, normally with some millimetres over an aqueous solution. As it was a DC plasma, the discharges can be either a positive discharge (PD) or a negative discharge (ND). The plasma jet has a wide usage field and one of those, for example, is the Graphene Quantum Dots (GQD) production by electric discharges. For better comprehension and more efficient production, the research of the plasma jet subject is interesting for the field of chemistry. For this reason, knowledge of the exchange surface between the plasma and the solution could cooperate to a better determination of chemical species transfer and the probed solution volume when using an absorption diagnostic.

So, to analyse the surface of the liquid in interaction with the plasma jet, a Synthetic Schlieren method from *Moisy et al.* [3] has been implemented and used to observe the disturbances and deformations. Comparing the images with shadowgraph images, the surface topography results have shown a good reliability in this application. For the usability of the method, the imperfections in the nozzle of the capillary tube, also called here by "needle", were used for the method. An additional irregular dot pattern was fixed in the needle with a PVC support.

For the surface analysis, the deformations were present with or without plasma. For

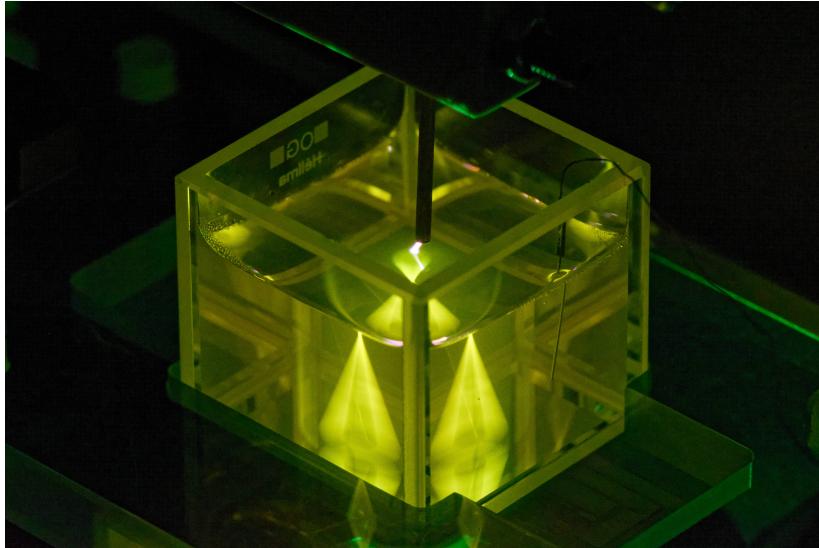


Figure 1.1 – Water solution in a glass recipient, the argon capillary tube, the platinum electrode and the discharge.

experiments without plasma, only the gas flow rate, the electric field and the voltage signal have been studied. The argon flow rate was set from 0 Standard Cubic Centimetres per Minute (*SCCM*) to 30*SCCM* and the tensions were up to 4500V. A combination of gas flow and electric field was also studied.

The method was also used when the plasma was ignited, the goal was to understand the distortions caused by the two polarities discharges. For the ND, a gas flow rate and an electrical current study has been completed. Still for the ND, a statistical surface has been calculated for each configuration and its deviation in time. However for the PD, it was impossible to perform a detailed study as the one made with ND, because of the hectic nature of the PD, although some observations could still be made.

2 BIBLIOGRAPHY

This section starts by defining the proper object of study, the plasma. According to *Bitencourt* [1] it is, from a scientific point of view, the fourth state of the matter, but differently from the others three states, it is not defined by the strength of bonds or has a similar nature for phase transition. A gas that receives enough thermal energy starts to dissociate into atomic gas and, if the temperature is high enough, the atoms starts to ionise. That corre-

sponds to the start of the plasma formation, or ionised gas. Furthermore, this transition from gas to plasma is not a step, it happens gradually with increasing temperature.

Other than by temperature increase, plasma can be produced by other ways. Two examples are: photoionization and the application of an electric field. In the last one, a high voltage is applied to a small distance and that generates a strong electric field, capable of accelerating the free electrons of the gas. The accelerated electrons in the gas reaches energies sufficiently high to ionise other atoms by collision, and generate the *Townsend* avalanche. That avalanche of electrons occurs when the free accelerated electron collides with an atom that provides another free electron, which in turn accelerates and collides with other atoms, increasing the quantity of free electrons in the mean and, consequently, increasing the chances of collisions in a factor of two. This electric field capable of promoting an electron avalanche has an order of kV/cm and for example, at atmospheric pressure air, the value is around $31kV/cm$.

That process provides free electrons capable of creating a current in the circuit if the electric field is maintained. Due to higher mobility, the electrons gain a lot more energy than the ions and then the electron's temperature becomes higher than the ion's temperature. Regarding the temperature, the discharge can be separated in two classes, cold plasma and hot plasma. Cold plasma refers to when the electron's temperature is higher than the ion's, as it is in this present example. On the other hand, hot plasma occurs when both temperatures have a similar value.

So, as previously described, a strong electric field is capable of generating a cold plasma and now, with that highly ionised gas, many applications are possible. Depending on the importance of which phenomenon, its applicability can be from power generation and flow control, to chemical reactions promotion. For the last one, essentially, those free electrons and ions are capable of accelerating chemical reactions or even enabling a non spontaneous reaction to occur. Hence, in a chemical application, a faster yield of a product or even a difficult reaction can be possible. A normal configuration for this application is to create the plasma in water or in the surface of water due to its faster reaction rate, that provides more encounters because of its higher density. Furthermore, water is a medium where the products can be reserved after the reaction in a simpler and more efficient way than in air.

In the oldest studies, the plasma jet field had a more chemical point of view, as observed in *Bruggeman et al.* [4]. There are articles and information available for the reactions, free radicals and substances present in the plasma discharge. The region in between the gas and the liquid is called interface and it is where a big part of the reactions take place, as seen in figure 2.1. The modelling of all these reactions is covered by *Van Gaens and Bogaerts* [6], which has a big quantity of data for substances and reactions along time and distance from the electrode.

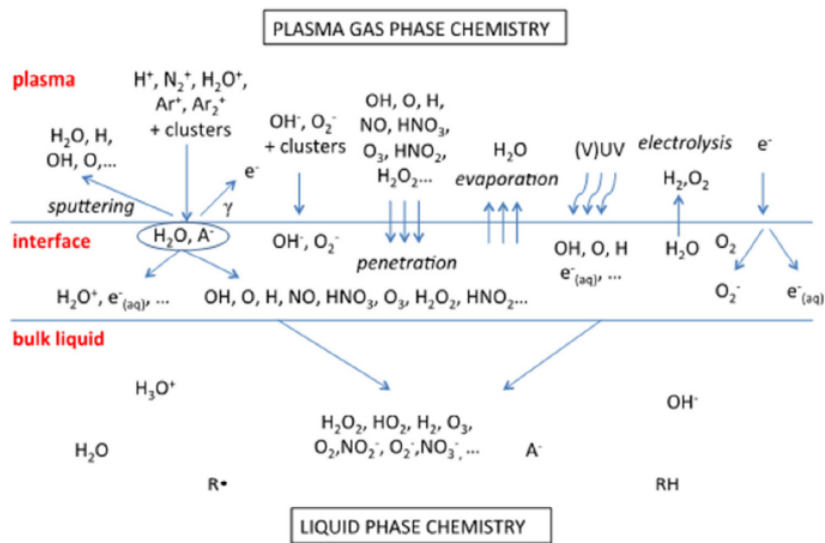


Figure 2.1 – Chemistry involved in a plasma discharge over a liquid surface. Figure 1 from *Bruggeman et al.* [4].

Although the fluid part was not largely studied, it has begun when *Holgate et al.* [5] started to see, in his problem of a magnetic fusion devices, the necessity of modelling the liquid lithium surface sheath protection stability in the plasma region. So, for that, numerical simulations have been run to observe the instabilities of the liquid surface. As seen in figure 2.2, initially there is a normal circulation, but when the instability comes in a certain system configuration, a higher protuberance appears and a droplet is formed.

In other papers, the plasma jet has gained more attention from the fluid mechanics perspective. Among the existing methods to experimentally analyse the fluid dynamics, the Particle Image Velocimetry (PIV) and Schlieren visualisation are two of them.

PIV is a 2D or even 3D optical measurement method that tracks particles between frames and returns the velocity field. In *van Rens et al.* [7], the flow behaviour inside the fluid

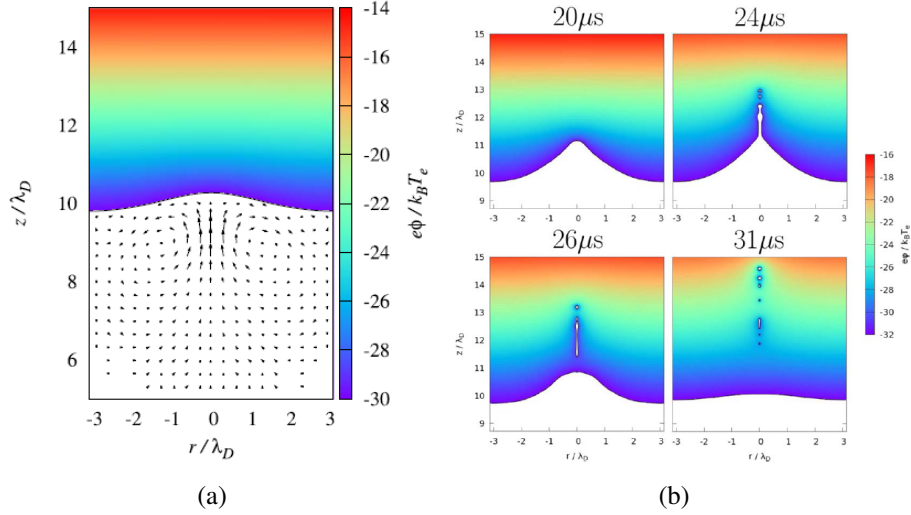


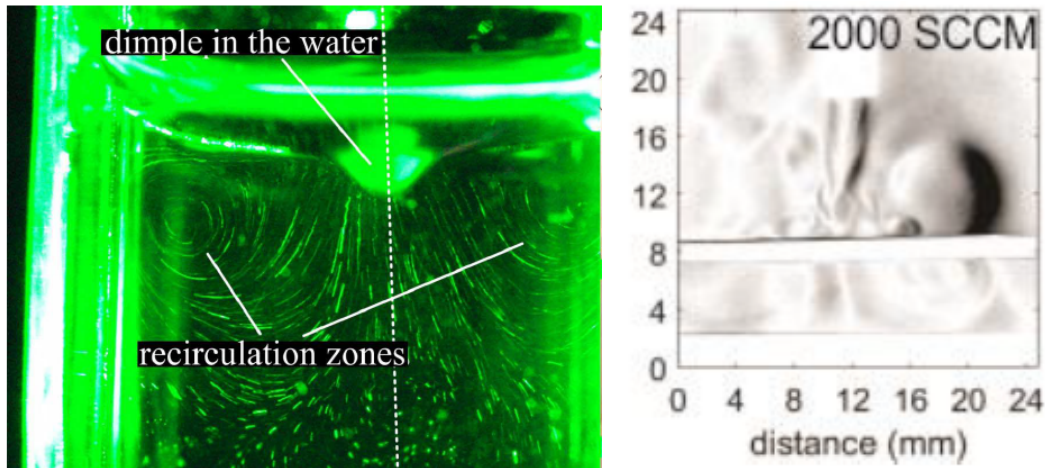
Figure 2.2 – The figure (a) shows the normal circulation in the plasma-liquid interface and the figure (b) shows an instability that grows and becomes a droplet. Figures 1 and 2 from *Holgate et al.* [5].

have been studied through this method. The argon flow deformation was also observed and analysed, both with and without plasma. In figure 2.3(a), the flow patterns inside the water and the dimple are observable.

The Schlieren method works with the non-continuity of densities in the medium and, consequently, of the diffraction index, which generates an image where there are darker and brighter areas. Using this other method for the outside part of the plasma jet system, the air phase was studied by *Kovačević et al.* [8]. This study saw the flow above the water, while changing the gas flow rate. It showed that, when the plasma is ignited, the gas flow changes. However, their work was carried out with an AC plasma, in contrast with the present study, which was done with DC. Therefore, we can not compare directly the results, but only take into account their observations regarding the flow.

So, looking for GQD production, *Orriere et al.* [2] used an argon micro plasma jet over a deionised water solution. He studied the discharges in a DC configuration and observed that the PD are more efficient to produce GQD than the ND. The two discharges have shown different deformations in water surface.

So, in order to sum with the plasma jet studies, the induced perturbations on the surface were observed and analysed in this report. To accomplish that, a method of "Free-Surface



(a) Flow inside the fluid induced by argon plasma jet. (b) Gas flow in the water surface induced by helium plasma jet

Figure 2.3 – Flow pattern in water and outside water. Figure 2 from *van Rens et al.* [7] and figure 14 from *Kovačević et al.* [8].

Synthetic Schlieren" (FS-SS) [3] has been used, as already mentioned in section 1. As *Moisy et al.* [3] explained in his paper, this method can be seen as a powerful tool to describe 3D surfaces from 2D images by taking into account the displacement of a pattern caused by air-liquid diffraction.

The FS-SS is not the only way of calculating a surface topography, since it is possible to use a more mathematical approach, in opposition to the Digital Image Correlation (DIC) procedure used for FS-SS. The other option is by a deformed regular chequered pattern via fast Fourier demodulation, for which the explanation is present in *Wildeman* [13]. Although the method is really efficient, the micro-scale of the chequered pattern needed for the lenses setup was really difficult to achieve. Even with the micro-engraver and the available printer, they did not have the required resolution. So, it was considered a better option to print a non-regular pattern and use the FS-SS method, which has shown good results.

3 METHOD

The FS-SS is a well known method and is, technically, a non-intrusive method for an instantaneous two-dimensional measurements. For the surface study, the method was applied

in a deformed pattern caused by the surface topography. In order to validate the method, the results coming were compared with lateral images of the interface deformation. Those images were taken by a shadowgraph montage that will be covered in subsection 3.2.

3.1 FREE-SURFACE SYNTHETIC SCHLIEREN

The FS-SS is composed by two steps, the correlation of the displacement field and the reconstruction of the surface by the integration of the displacement field. To obtain that, a DIC code must be used and there are a lot of options, also for free. For this study in special, the most used was *PIVlab* ([14],[15],[16]) and some uses of *DaVis*. For the reconstruction part, the integration is based on the least-squared inversion of the gradient operator.

For better comprehension, the experimental setup is shown in figure 3.5. It consists of a water recipient that was positioned below the plasma. The nozzle of plasma jet needle imperfections and even a support for a pattern were illuminated trough the water and seen by a camera and a lens configuration. And when the surface was perturbed, it changed its shapes and deformed the pattern.

With that in place, it became possible to observe all the perturbations in the pattern above the water by comparing the image with a reference image as seen in the figure 3.4. To convert this in heights, an initial height between the pattern and the initial surface is needed. To obtain the value, it was used a shadowgraph method, that calculate it. The height is an important step of the method in order to have a good resolution and for the calculation itself, but it also has some limitations. If the space between the parts is too wide, the ray crossing phenomenon can happen and ruin the sample. Even if this phenomenon does not occur, a huge space can also be difficult to correlate and the gain in resolution is lost in regions with stronger curvature.

An important remark is that the explanation given in the next paragraphs is for a pattern in the water side and a camera in the air side. Even though the used setup in this work is inverted, the calculation process does not change.

The mathematical process is not complicated and can be simplified. The initial point is

to know that the reference image is already deformed because of the field of view, so the region far from the centre of view has already a displaced position that is caused by paraxial angle. This problem is approximated by placing the camera far from the pattern and the distance could be considered infinity if compared to the distance between the pattern and water surface. The second approximation is called weak slope approximation, that simplifies the displacement of the point for a 2D shift. And the last one is weak amplitude approximation, that says that the mean height is bigger than its variation.

In the next figures, it is possible to understand the mathematical process and approximations. The figure 3.1 shows that even with a flat surface, the point M is already displaced to the point M' .

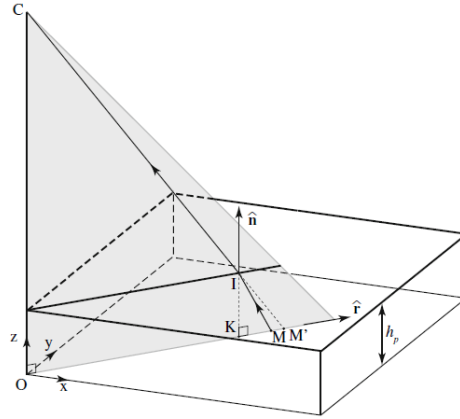


Figure 3.1 – Paraxial approximation, the point M has shifted to M' but when taken into account the camera-pattern distance to the infinite, the angle goes to zero and it can be neglected. Figure 1a from *Moisy et al.* [3].

From figure 3.2, it is observed that, with weak slope approximation it becomes possible to use small θ and simplify the normal vector. In addition, with the paraxial approximation the normal vector can be written by equation 1. So, the equation 2 can be written by subtracting from z (see figure 3.1) the normal \hat{n} (figure 3.2 and equation 1), and by performing some variable changes it will arrive in equation 3.

$$\hat{n} = i\hat{s} - \frac{CM''}{|CM''|} \quad (1)$$

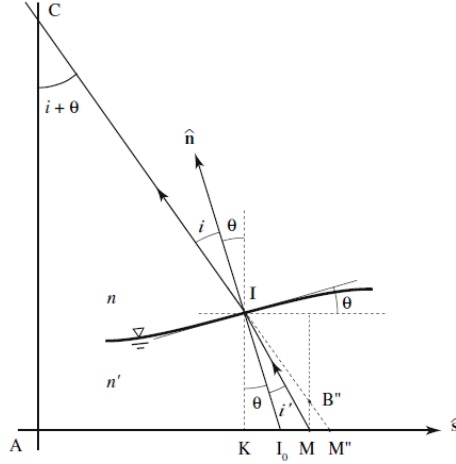


Figure 3.2 – The angle between the normal vector and the vertical is θ and with weak inclinations, θ could be small and simplify equations. Figure 2b from *Moisy et al.* [3]

$$\nabla h = z - \hat{n} \quad (2)$$

$$\nabla h = \frac{OM''}{H} - \frac{MM''}{\alpha h_p} \quad (3)$$

Equation 4 results from the decomposition of $OM'' = OM' + \delta r$ and $MM'' = MM' + \delta r$ where $\delta r = M'M''$ and $MM' = \alpha h_p i \hat{r}$. Here, ∇h is the surface gradient, δr is the displacement field, h_p the pattern-surface height, α is $1 - \frac{n}{n'}$ where n are the refraction index, and the final one, H is the camera-pattern distance. That equation can be integrated numerically.

$$\nabla h = -\delta r \left(\frac{1}{\alpha h_p} - \frac{1}{H} \right) = \frac{-\delta r}{h_*} \quad (4)$$

$$h(x, y) = h_p + \nabla^{-1} \xi \quad (5)$$

So, after all these steps, the height value is obtained by equation 5 by opening the discrete system in second-order centred difference. With $\xi = \frac{-\delta r}{h_*} = \xi_x \hat{x} + \xi_y \hat{y}$ the system is over-determined, but, without that, it is not possible to totally reconstruct the surface because the original system was a vectorial and now it becomes scalar. So, a solution is defined by imposing the reference height for the first cell and by searching for the "best" solution in a

least-square approach, minimising the residual $\|\nabla h - \xi\|^2$.

Thus, the solution from the equation 5 is the height in every cell for the discrete field. And after that, it is possible to reconstruct the surface topography. More details are deeper explained in *Moisy et al.* [3].

3.2 SHADOWGRAPH

The shadowgraph is a simple experiment to see the deformation. That method was used for the validation process by comparing images. A profile image of the deformation was captured, figure 3.3, and was compared with one of almost the same instant FS-SS result surface. The shadowgraph is limited because it requires the water level to be at the top of the container (due to the meniscus) and only sees outwards deformations, so for the validation process a surface deformation caused by a negative electric field was used.

A second use of the shadowgraph was to calculate the initial height of the surface. By knowing that the capillary tube has $1,7mm$ in diameter, the pixel distance was converted in mm and now, with a non-deformed surface, the distance between the water level and the nozzle, or the pattern support, could be taken. That method was a good option for taking the distance pattern-surface.

The use of this method is also possible to observe the non-uniformity in the transparent means like water or air. For example, a density variation in air changes its diffraction index. It is seen in the images as a darker or brighter areas because all the light rays trespassing the experimental section. Those light rays are expected to be parallel, but if there is a non-constant diffraction index, they deviate and create those areas of changed brightness.

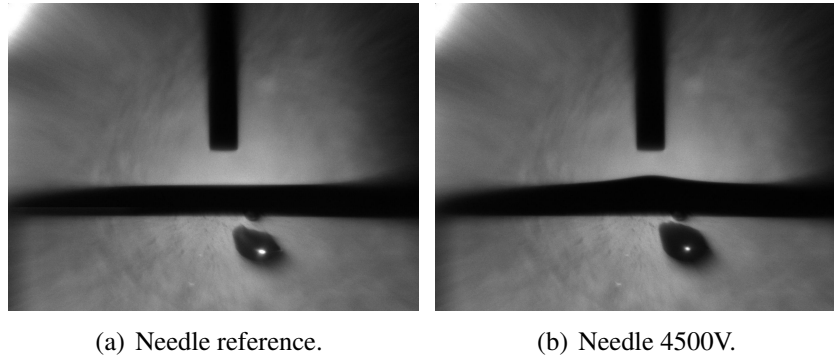


Figure 3.3 – The shadowgraph is capable of seeing the protuberance formation in water surface that creates that magnifying less effect. Here it is shown the plasma needle, the water surface and the glass container. The figure (a) is the reference one without the electrical field.

3.3 EXPERIMENTAL SETUP

In the figure 3.4, the image of the nozzle is shown in a configuration with electric field to observe the changes in comparison with the reference one. Those images were treated in DIC and its displacements fields were converted in heights in the FS-SS code. With the raw images, it is already possible to observe that, with an increasing tension, the deformations become progressively stronger. From the first one to the last one it is possible to see a magnification of the nozzle that was caused by a protuberance in water surface. That surface bump is shown by shadowgraph in figure 3.3 for the $-4500V$ electric field.

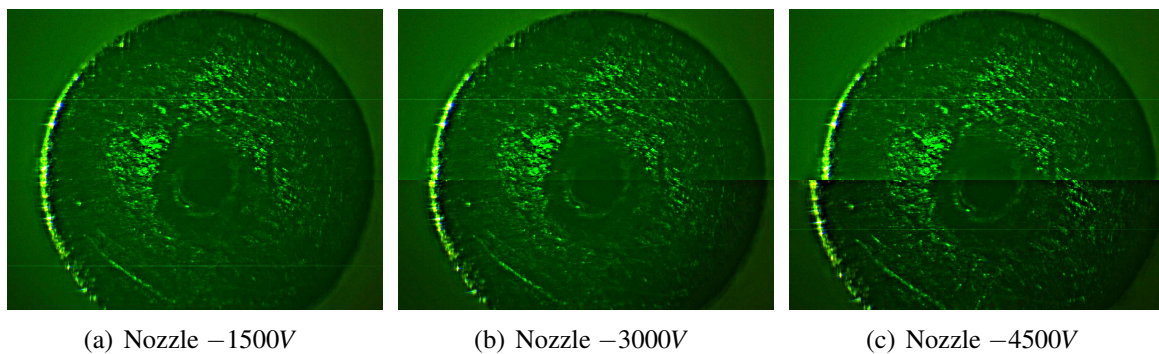


Figure 3.4 – The magnification seen in the bottom half of each images after an augmentation of voltage if compared with the reference in the upper side. From (a) to (c) only the voltage has been changed.

For the images in figure 3.4 and the other steps of this method, some equipment were

needed, as shown in figure 3.5 and 3.6. For the FS-SS, the light source was a green LED Luminus CBT-120 controlled by a signal generator Armixel PDG-2520. The camera used was a THORLABS DCC1645C. The lens setup also shown in figure 3.5 was composed by a zoom lenses pack with a 200mm and 75mm focal distance lenses. In the camera side, a 200mm lens was placed and for the light side, 300mm, 75mm and 30mm lenses were placed to be able to focus above the camera focus plane illuminating the entire field of view. To enable this collinear setup, a beam splitter was placed to see the illuminated field, but it reduces the brightness of the image. The water recipient was a Hellma Analytics Large Cell 704.001-OG with a cube of 30mm edges made in optical glass to see through the bottom of the container with minimal diffraction. An additional continuous white light source was mounted right beside of the water recipient for better illumination for the ND.

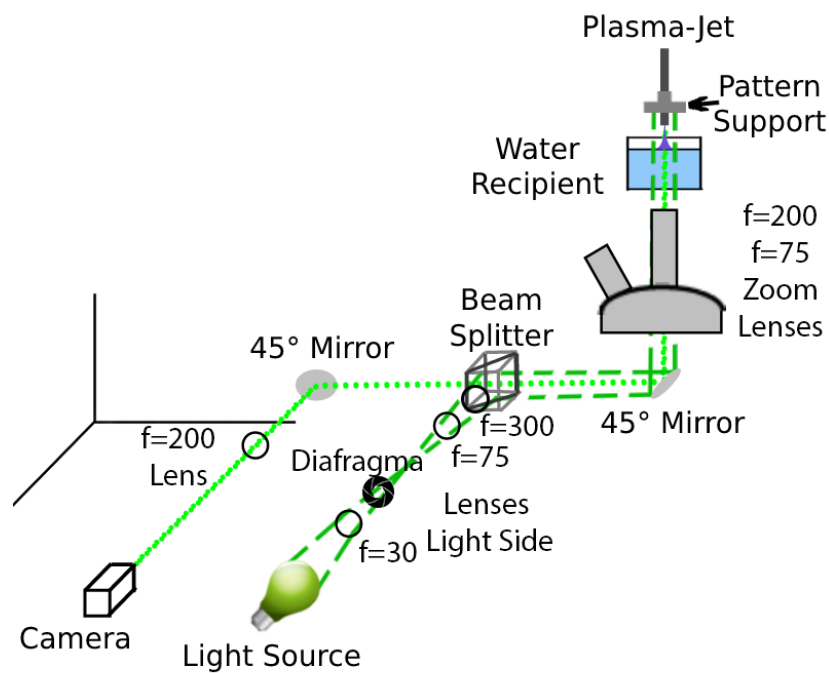


Figure 3.5 – Optical Setup for FS-SS.

The shadowgraph setup is simpler and was composed by a light source THORLABS QTH10/M, a condenser, a 1mm pinhole, a Point Grey FL3-U3-32S2M-CS camera and three more lenses. They were a 60mm focal length for the light side and for the camera side, a 125mm and 150mm focal length. The focal plane to the shadowgraph must be at the crest

of surface deformation and to achieve that, the distance between those two lenses in camera side were changed. All the equipment are shown in figure 3.6.

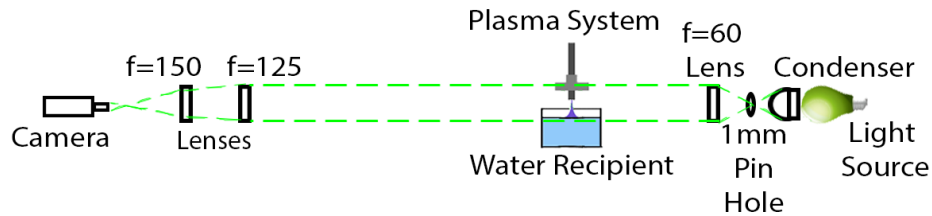


Figure 3.6 – Shadowgraph setup.

For the electric setup, a DC power supply from Stanford Research Systems Model PS 350 was connected via a ballast $150k\Omega$ resistor to the plasma jet needle electrode. The other side was grounded via shunt resistor of 50Ω connected to a platinum electrode. An additional system was composed by an oscilloscope that was connected to the ground side circuit by a coaxial cable, as shown in figure 3.8. The plasma jet needle was a metallic tube of $1,7mm$ of diameter with a hole of $180\mu m$ of diameter and argon flowed through this tube from a bottle, at a maximum $30SCCM$.

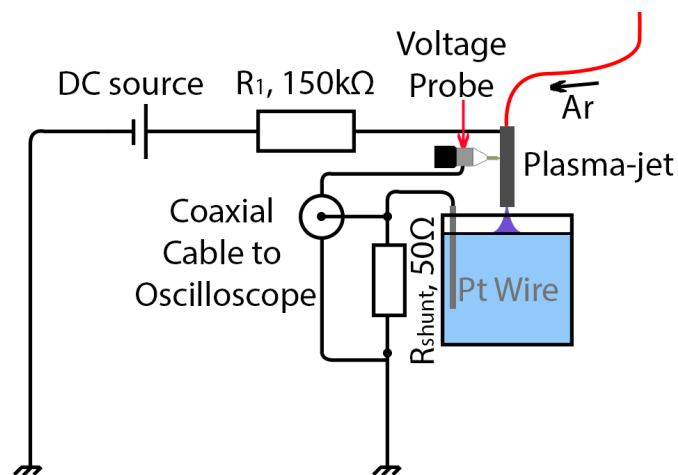
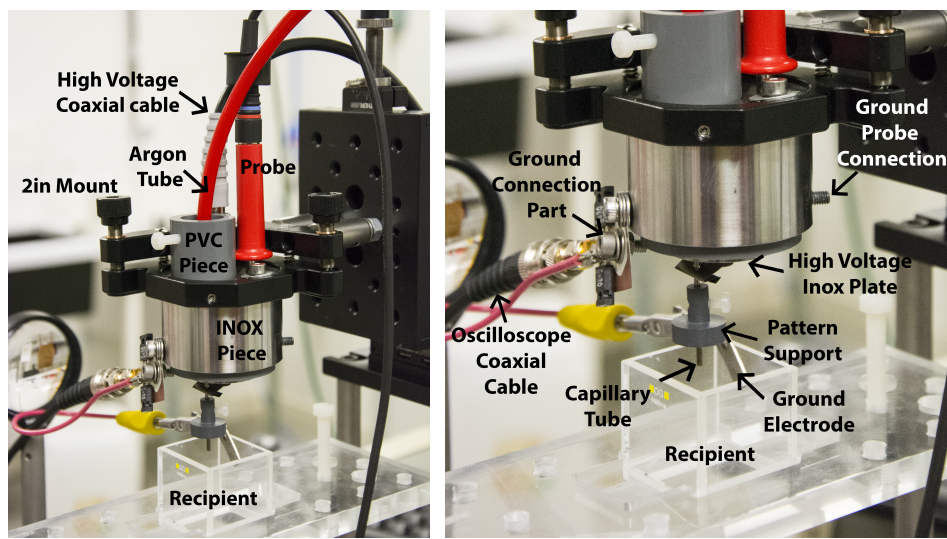


Figure 3.7 – Electric setup of the microplasma-jet.

To organise all that, the high voltage connection, the argon capillary, the voltage probe and the ground side, a composition of a PVC and an INOX components have been conceived. The PVC part provides stability and isolation for each component and it was mounted inside the INOX shell. This last part provides a good connection between the platinum electrode circuit, the ground part of the probe and the power supply ground. In the bottom part, an INOX small plate provides contact between the capillary tube, the high voltage connector and the test probe. The platinum electrode was connected via the shunt resistor and to the oscilloscope via a coaxial cable for electrical current monitoring.



(a) Probe, high voltage, argon tube and recipient in the PVC/INOX mount. (b) Pattern support, ground connection, capillary, platinum electrode and other parts.

Figure 3.8 – Mechanical mount for the study.

3.4 PARAMETERS AND TREATMENTS

For the validation and the majority of the remaining results here, the parameters used for the experiments were set the light to shine with the frequency of $5Hz$ for $20ms$. Exceptionally for the PD, the LED period was also decreased to $5ms$, in order to obtain sharper images. Also, the camera was configured to have the same frequency as the light in order to synchronise and not superpose the light pulses. Moreover, the exposure time was set to be highest possible.

The images were captured and an increase in sharpness has been made for some images

in Photoshop with the filter Smart Sharpen. In the DIC program, the only image changes were a contrast enhancement and a mask application. For the correlation, a FFT window deformation algorithm included in *PIVlab* was used. The interrogation areas were $128px$, $70px$ and $40px$ and the steps were $70px$ and $40px$. The sub-pixel estimator chosen was a Gauss 2x3-point and the correlation robustness was set to high. In the post-treatment, the limited displacement was set to $40px$.

3.5 VALIDATION

The validation of the implemented method was necessary to confirm the results and see its reliability. To do that the height results were checked with the shadowgraph images. For this process, the plasma was not ignited, only the electric field was set in place. The deformation caused by that configuration was greater and more stable to compare. One important point to remark is that the two images, the one from FS-SS and the other from shadowgraph, have not been taken at the exactly same moment and may vary a little.

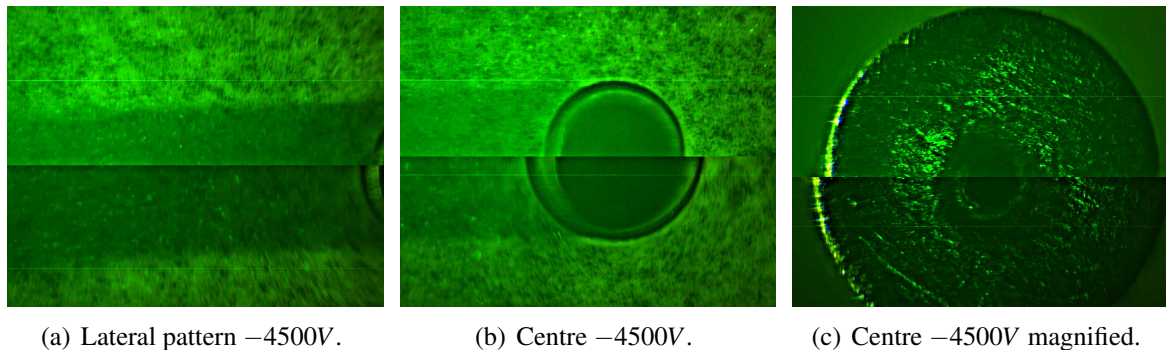


Figure 3.9 – These three pictures have on the top half the reference and the other part the deformed ones from an electric field generated by $-4500V$. The first one is the lateral part of the needle and it is possible to see the dot pattern used, in addition, the magnification of this lens is the same as (b). That image is the one with the smaller magnification at the centre and the (c) with the biggest magnification.

The process started with the images taken with two sets of lenses and positions. The post-process DIC calculated the displacement field, the initial height came from shadowgraph and the height field was calculated. The figure 3.9 shows the reference pictures and the deformed ones when the voltage was applied. For reference, the jet has $1,7mm$ of diameter.

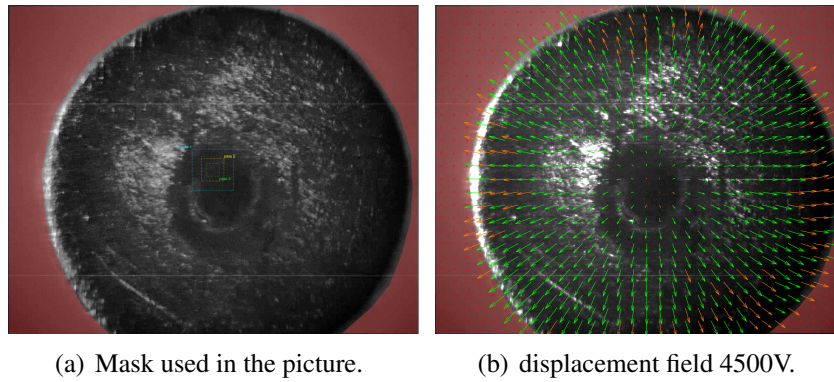


Figure 3.10 – Those images are the DIC process. In (a) is possible to observe the masks and the interrogation areas and in (b) the calculated displacement.

So firstly, the DIC has to be made and for that the software *PIVlab* was used. Outside the nozzle, the stronger magnifying lens did not capture any information, so it was masked, as shown in the figure 3.10. The first interrogation area, as said, was $128px$ with 3 passes and the last one was $40px$. So, to export the displacement field, it was calibrated with the reference image, by the known needle diameter of $1,7mm$.

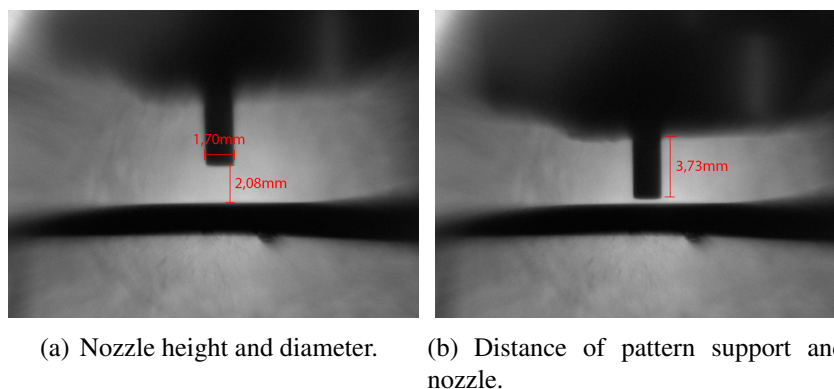


Figure 3.11 – Here the heights are shown and also the reference distance, the needle diameter.

To continue with the study, the initial height needed to FS-SS was calculated with the shadowgraph image, remarking that the nozzle and the pattern did not have the same height, figure 3.11. The needle diameter is $1,7mm$, so the height could be found using the diameter as a reference distance. With the height, the topography could be calculated and seen, as shown in figure 3.12. For the validation, the field was calculated with the three configurations, the lateral, the centre and magnified centre. Those three images were compared with the shadowgraph and a profile has been composed with the three lenses.

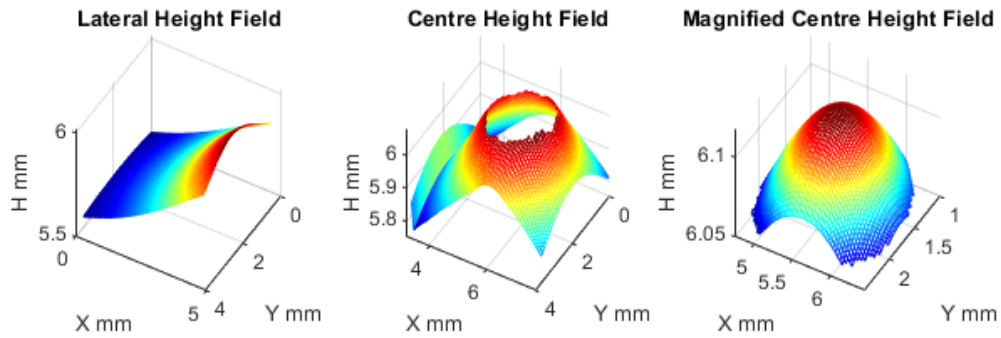


Figure 3.12 – The height field in each lenses and positions.

As seen in the figure 3.13, the profiles were close to the shadowgraph image and they could affirm that the results from the FS-SS method and code were reliable. The value of height was not as correct as it had to be. That occurs because of the integration process where the reference height was smaller than the minimum height after the deformation, so the entire field was placed at the initial height, however the shapes were, as seen in the figures, correct.

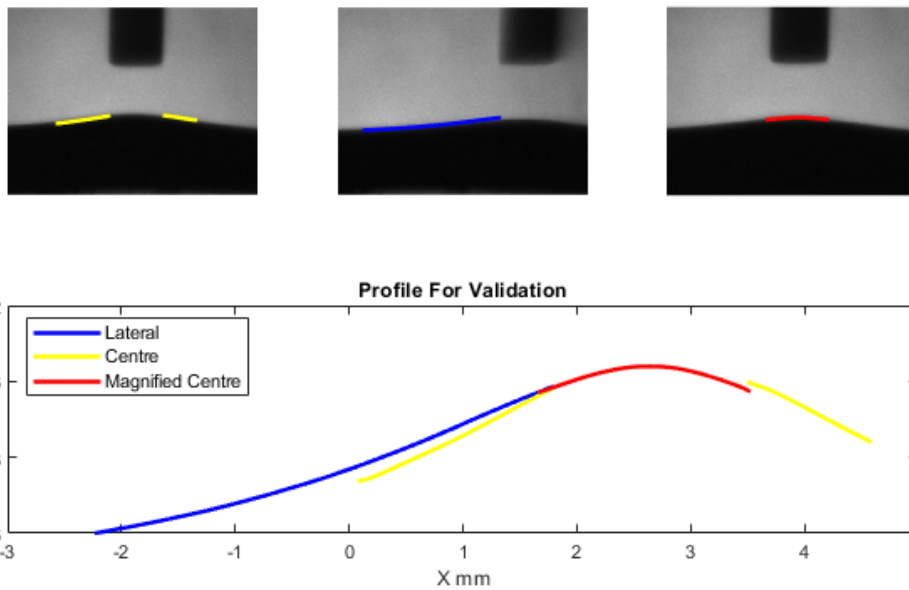
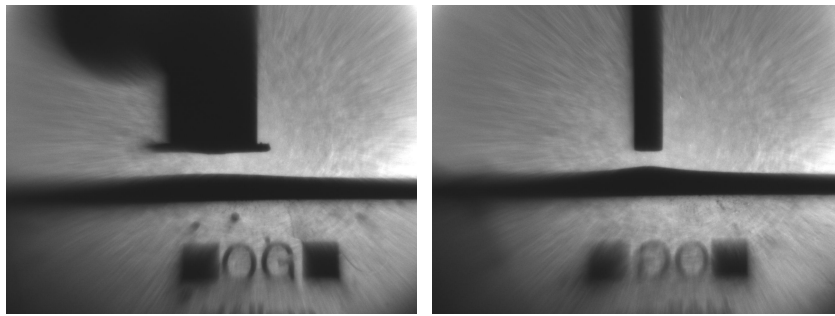


Figure 3.13 – Those three images show the profile taken in the highest point. The middle one has been taken in the lateral, the right one has the same frame as the left but it is magnified. In the bottom is placed the three profiles in the same composition. The yellow curve has a mask so there are not results in the middle part.

So, according to the validation, the data taken from FS-SS were reliable especially only considering the shape of the deformation.

3.6 LIMITATIONS

Although the FS-SS has strong results, it still has its limitations. As already pointed out, the ray crossing and the difficulty of correlation are two of them. However, they are not the only ones. Here it is possible to remark a different deformation when the pattern support was placed in different positions, as shown in figure 3.14. It is not interesting for the study because the method, *a priori* non-intrusive, changes the results for a real application without the pattern addition. In general, when the support was really close to the nozzle, the deformation was wide, but, when it starts to move away from the nozzle, the protuberance became more pointed and then, when it was placed further, it decreased again. Nevertheless, when the support was right in the nozzle, the plasma ignition was really difficult and almost impossible to achieve. The circuit tripped itself or the water touched the support and the circuit tripped again.



(a) Pattern support right over the nozzle creates a smooth protuberance. (b) The same voltage as (a) but without the support.

Figure 3.14 – Differences in the surface because of the electric field perturbation caused by the pattern support position.

A greater distance was envisaged to improve resolution and to have the least possible perturbation, but the bigger the distance, more difficult it was to correlate the images. As shown in figure 3.15, the difference in pattern-surface distance generated a stronger deformation as it went higher and the blur made the correlation impossible. For small deformations high distances are interesting but stronger deformations require smaller distance.

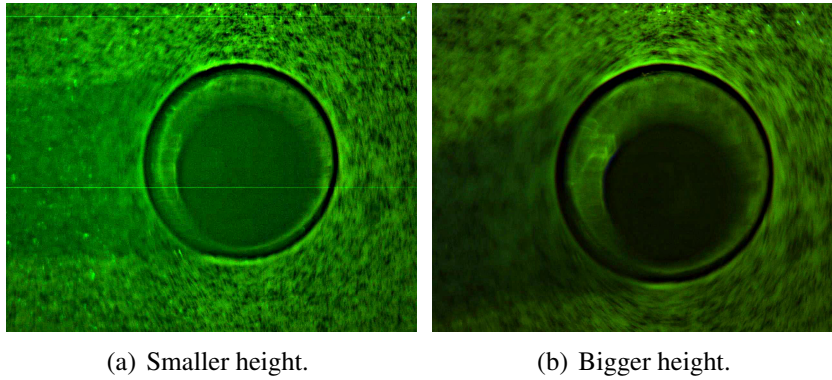


Figure 3.15 – Two pattern surface distances for a same electric configuration.

Because of all those points, the pattern support was placed with a distance of around 5mm from the bottom of the capillary tube. With that, the lens with the greater magnification, proposed to see the nozzle, and the other one have two different focal planes and that was why the areas out of focus were masked. In consequence, the field and profiles from figures 3.12 and 3.13 had an empty part for some optical configuration. Consequently the full fields were composed by two different topographies and the link between them are not perfect to show, however if they were seen separated they are suitable to be analysed.

4 MEASUREMENT WITHOUT PLASMA

In this section the application of the FS-SS was to study only the system without the plasma ignited. In a first time, voltage was applied to the metallic tube and consequently the surface of the liquid was attracted due to the electric field. In a second time, a gas flow was also studied, separately and with the voltage application.

4.1 NEGATIVE VERSUS POSITIVE DEFORMATION

For this comparison, the selected tension was $\pm 3000\text{V}$ and the negative electric field deformation was compared to the positive one. The height calculated from a shadowgraph image was $1,565\text{mm}$ for nozzle height and $5,551\text{mm}$ for the pattern height. As seen from figure 4.1, the differences in shape deformation were not sufficient to identify discrepancies

between the positive or negative polarity.

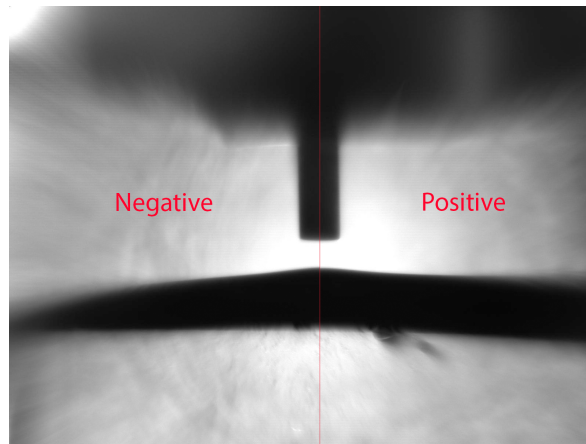
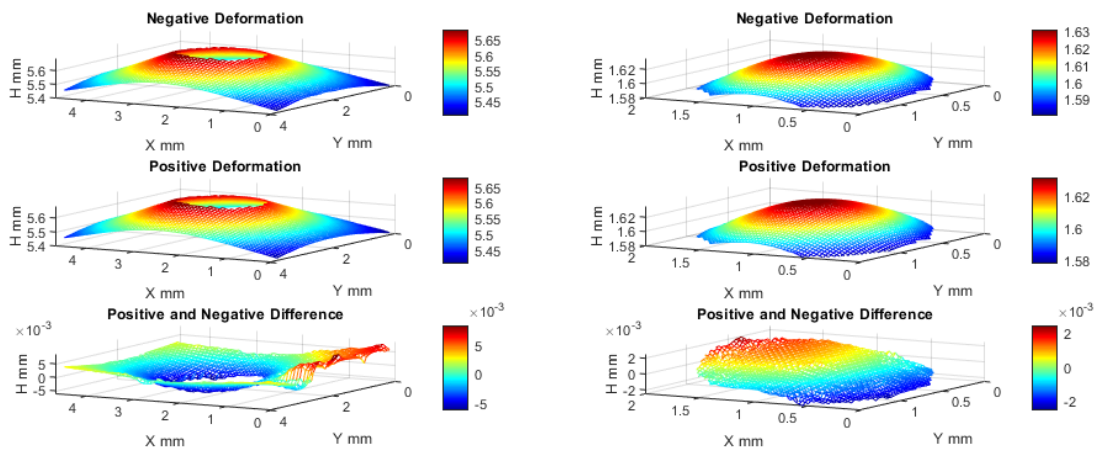


Figure 4.1 – In the left there is the deformation caused by a negative tension and in the right caused by a positive tension.



(a) Smaller magnification lens.

(b) Greater magnification lens.

Figure 4.2 – Negative, positive topographies and the calculated differences between each one.

In the FS-SS result, in figure 4.2, the two topographies were similar and the differences between each other were minimal. Those variations were too small to affirm that the change in polarity was the cause, because between the pictures there was still evaporation and other movements, which was probably the sources of the discrepancies. From the graph *Positive and Negative Difference* in figure 4.2 (a) and (b), among the positive and the negative the biggest discrepancy was of only $5\mu m$.

4.2 NEGATIVE AND POSITIVE VOLTAGE STUDY

Continuing without the plasma, it was studied the effect of various voltages in the system without igniting it. The height of $2,236mm$ was set then a negative voltage of $-4500V$ could be applied to the tube without plasma ignition. So starting from $-4500V$ to zero in steps of $1500V$, it was possible to understand the variation behaviour. The figure 4.3 shows that, as the tension was increased, so was the height. And it is possible to see that it is probably non linear with the voltage, because as the tension is increased, the electric field gets stronger and pushes the water up, but at the same time the distance decreases and makes the electric field even stronger.

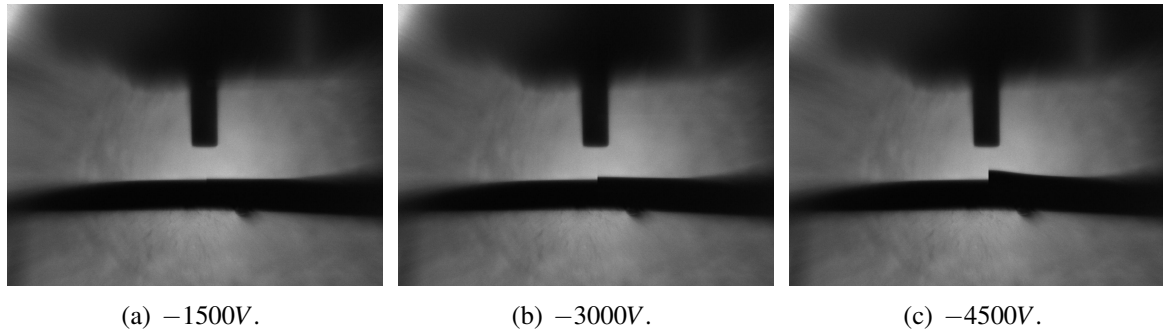


Figure 4.3 – Shadowgraph images of different tensions. The half left part of the images are the reference and the right is the deformed ones.

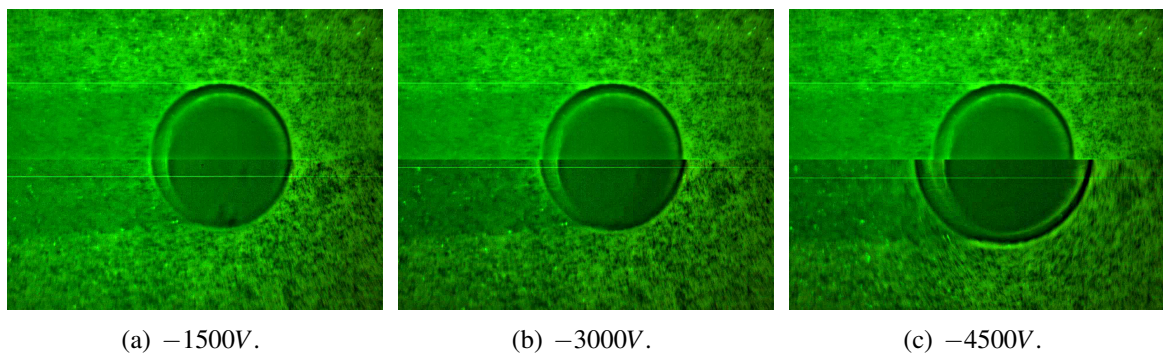


Figure 4.4 – FS-SS images of different negative tensions in centre position with the less magnifying lens. In the top part the reference half and in the bottom the deformed ones.

The resulting surface had radial symmetry, as expected, and the profile evolution is seen in figure 4.5. It had not a linear behaviour and it had a teardrop pic as *J T Holgate et al* [5] saw in his simulation. The nozzle and pattern heights for figure 4.5 were $2,236mm$ and

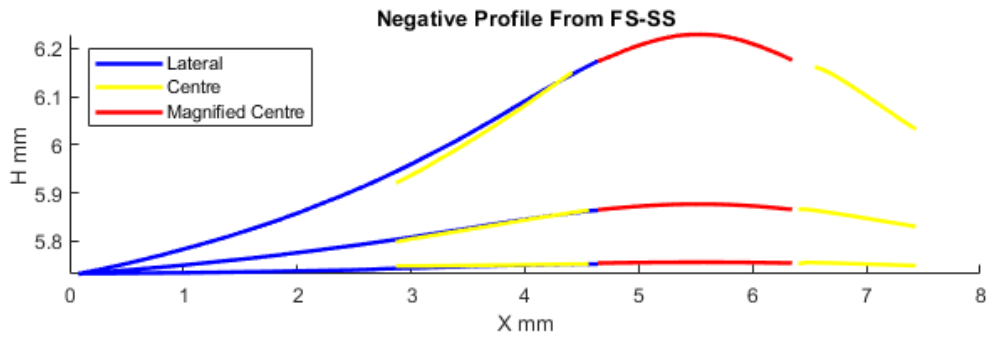


Figure 4.5 – Profiles observed via FS-SS for $-1500V$, $-3000V$ and $-4500V$. The highest one is for $-4500V$ and the lowest for $-1500V$.

5,741mm and the result shown had the start point altered to begin exactly at the same point.

The results for the positive tension had the same characteristics. Also, as seen in subsection 4.1, the differences between both polarities were minimal and did not make important differences in this study. In figure 4.7 it is possible to confirm the resemblance. The differences were results of the placement in the pictures, especially for the *Centre*.

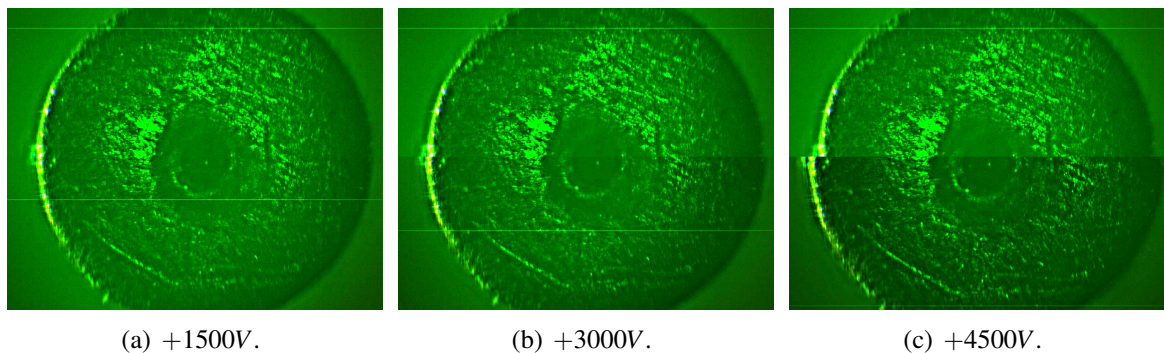


Figure 4.6 – FS-SS images of different positive tensions. In the top part the reference half and in the bottom the deformed ones.

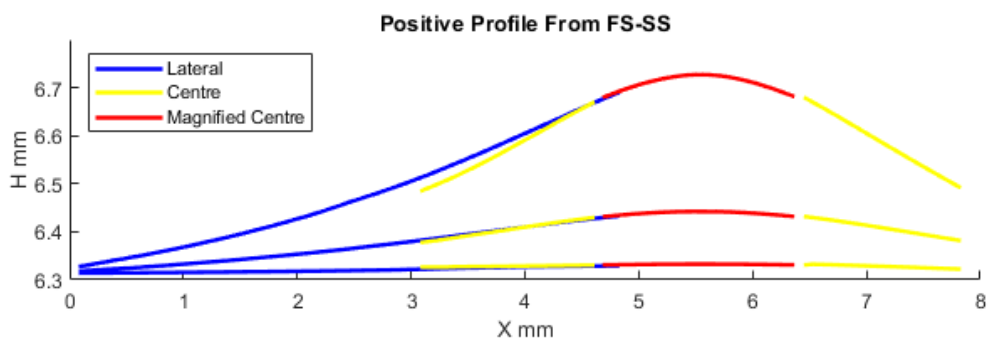


Figure 4.7 – Profiles observed via FS-SS for $+1500V$, $+3000V$ and $+4500V$.

4.3 GAS FLOW RATES

The plasma jet was used with a gas flow of argon to help to stabilise the arc. To this flow, the normal operation rate here were 25SCCM, the same used in *Orriere et al* [2]. In this section, only the flow rates were seen and the resulting deformation. So, in order to understand more the behaviour, the flow rate was changed and the voltage was set to zero.

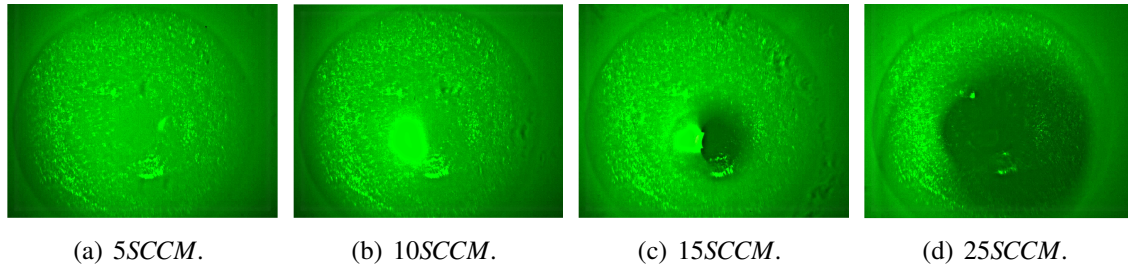


Figure 4.8 – FS-SS images of different argon flow rates without electric field.

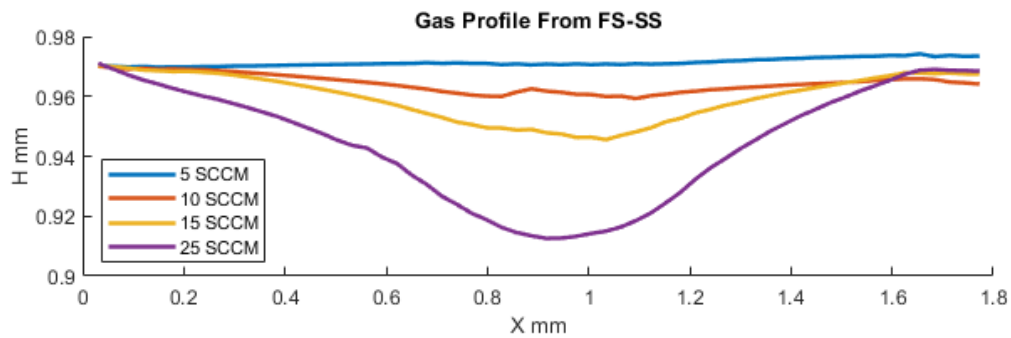


Figure 4.9 – Gas profiles observed via FS-SS.

The deformation corresponds a depression as seen in figure 4.9. This result is consistent with *van Rens et al.* [7]. In figure 4.8 it is possible to observe a brighter point in the centre as the flow rate was increased and it turned darker again probably because of the side illumination.

For more comprehension, the argon flowed at 25SCCM which corresponds to around 16m/s of speed. This exiting velocity was deviated within 1mm of height in agreement with what was seen in *Kovačević et al.*.

4.4 GAS FLOW RATES WITH NEGATIVE ELECTRIC FIELD

The negative electric field allied with the gas flow had a different perturbation over the liquid surface. It could be interpreted as the composition of the negative and the gas deformations, but it has shown that the system depends on the two parameters: electric tension and gas flow rates. It was maintained at $-3000V$ and the argon flow was changed from $0SCCM$ to $30SCCM$ in steps of $6SCCM$. The heights calculated from shadowgraph were $1,885mm$ for only the needle and $6,089mm$ for the pattern. For this study the height was also set to the minimum possible without the arc.

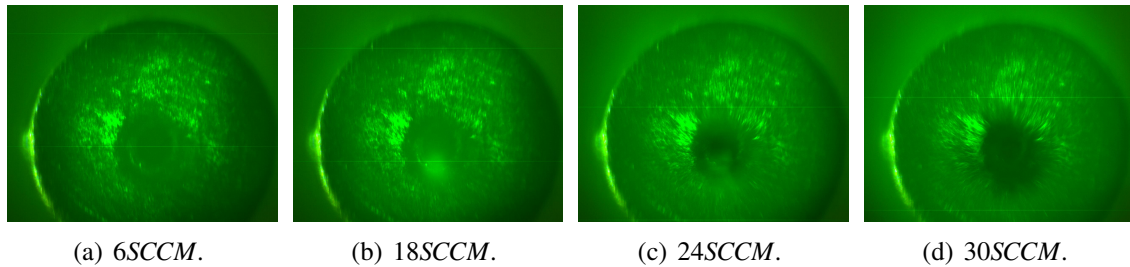


Figure 4.10 – FS-SS images of different argon flow rates with $-3000V$ in the amplified lens.

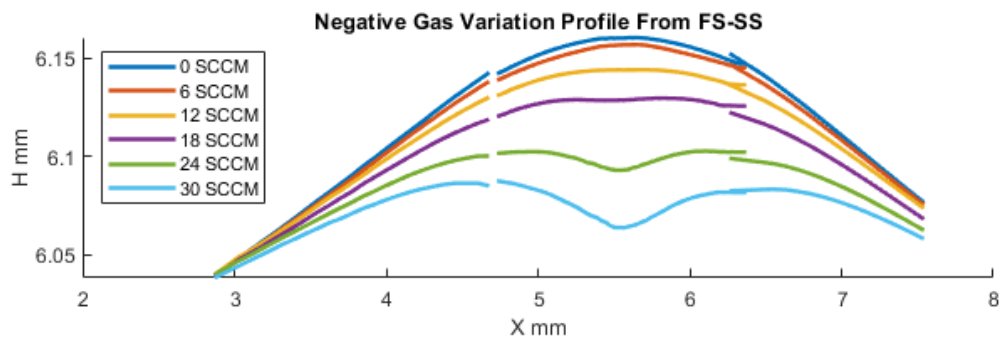


Figure 4.11 – Profiles observed via FS-SS for $-3000V$ and different flow rates.

For figure 4.11 the profiles were adjusted to start from the same point and it is possible to see that, as the gas flow rate was increased, the deformation started to change its shape. It decreased and created a depression right in the centre of the argon jet and even with the electric field pulling the surface upwards, the gas could deform the surface. The flow rate as high as $30SCCM$ generated a relevant force in the water contact that pushed it down again. For a scale idea, the fluid velocity was about $20m/s$.

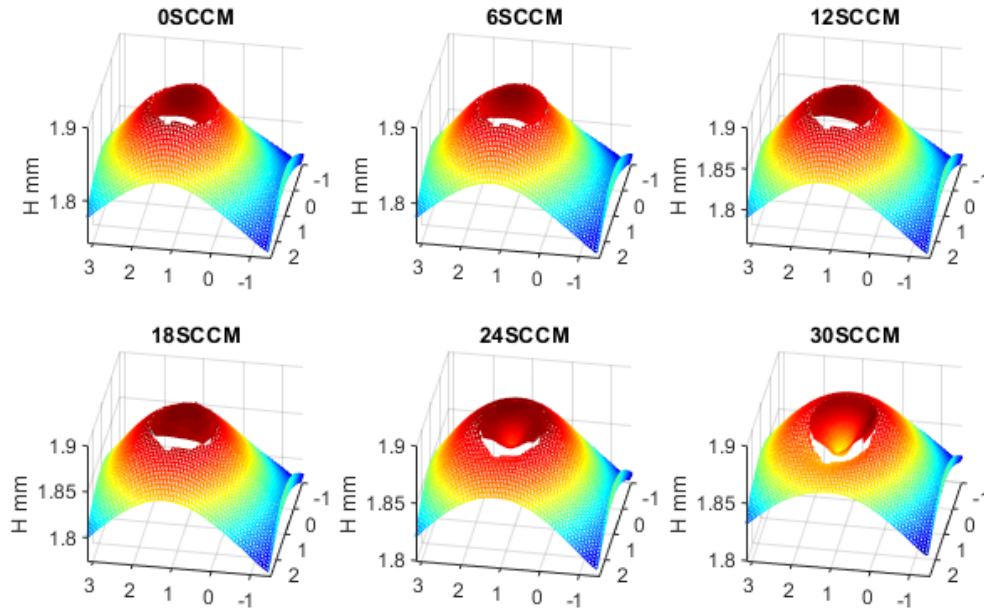


Figure 4.12 – The surfaces here are the corresponding surfaces to the profiles in figure 4.11.

In figure 4.12, the surface is similar to the profile. The protuberance decreased in height and a depression appeared when the flow rate increased as high as 24SCCM. The surface is not fully continuous because the data came from two different zoom lenses, and for the less magnified one, the mask covered part of the nozzle.

4.5 GAS FLOW RATES WITH POSITIVE ELECTRIC FIELD

As seen in subsection 4.1 the positive and negative electric fields have not had a big difference, however it was still studied with the gas flow variation. It is important to point out that even though the two results have had the same behaviour, the positive has shown to be more difficult to be established in the threshold height when compared to the negative. This observed difference could be caused by a difference in the water level due to evaporation, and chemical reactions after successive discharges. So besides the variation, in figure 4.13, it is possible to see the pattern deformation and, in figure 4.14, the profiles had the same shape as the negative, apart from the less pointy depression.

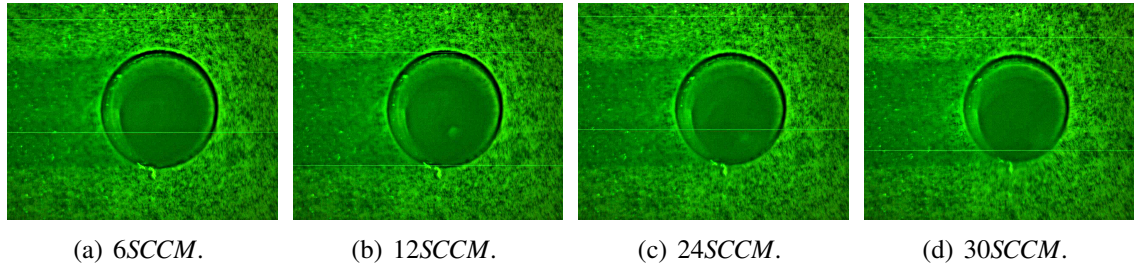


Figure 4.13 – FS-SS images of different argon flow rates with +3000V in the biggest magnification lens.

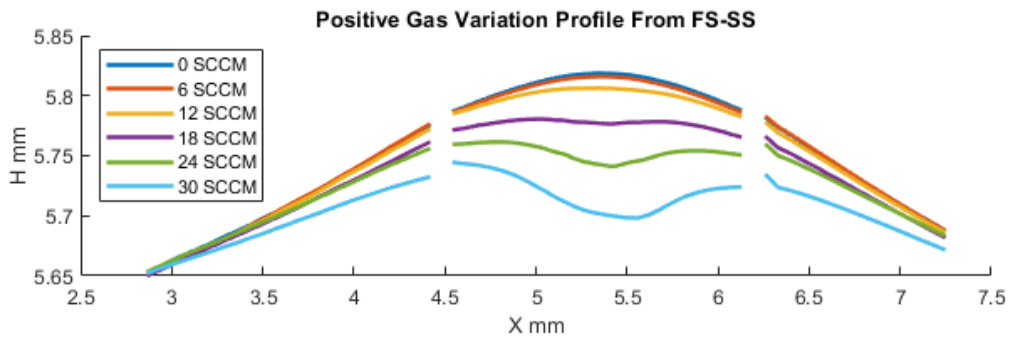


Figure 4.14 – Profiles observed via FS-SS for +3000V and different flow rates.

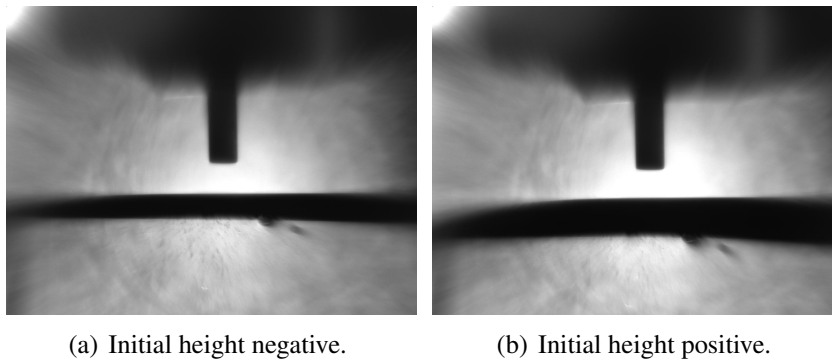


Figure 4.15 – Those images show the differences in negative and positive experiments. The negative one has less water than the positive and it stabilised taller than the positive.

As in figure 4.11, the behaviour of the positive deformations have had the same characteristics, it decreased in height as the gas flow rate increased. After 18SCCM, it started to invaginate and create a cavity right in jet's centre that went even deeper. However, as said, the invagination process looks less sharpen than the negative.

5 MEASUREMENT WITH PLASMA

This section will cover the plasma jet in function. The goal was to take the differences in negative and positive applications. Unlike the similar positive and negative polarities in not ignited experiments, here there were a lot of differences between the PD and ND. Those changes were so big that even turned impossible to make good assumptions about the PD.

To initiate, the PD had a lot more movement so a faster shot was envisaged. Thus, when the less magnification lens was used, the image was darker and impossible to correlate. In figure 5.1, it is possible to see that, for a PD, the bigger lens would not work and, because of that, the greater magnification lens was used for the next subsections. As shown in figure 5.2, that lens generated an image with usable information.

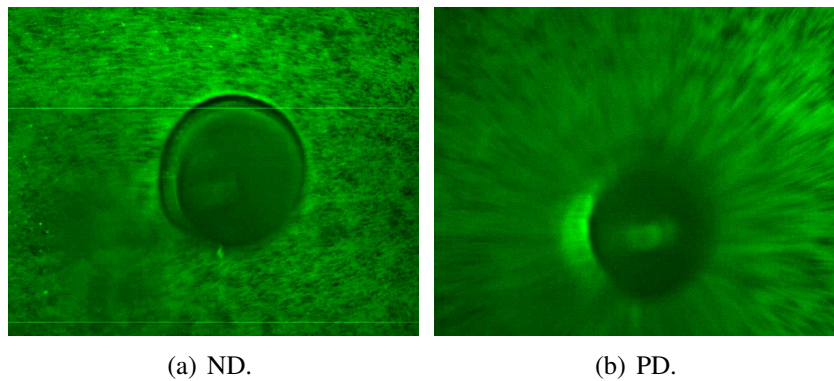


Figure 5.1 – Those images show the discrepancy in image information when the discharge polarity changes with the less magnifying lens. The initial voltage for both polarities was 2500V, the current was 3mA and the gas flow rate was 20SCCM.

Another statement of figure 5.2 is that the plasma had a totally different behaviour. In the PD it was just a small dot and for the ND it was stretched and not regular as the other one. A last point to mention is that, in the next FS-SS topography results in the following subsections, the area far from the nozzle must not be considered, because it was calculated by a faster code option that calculates a height also to the masked area.

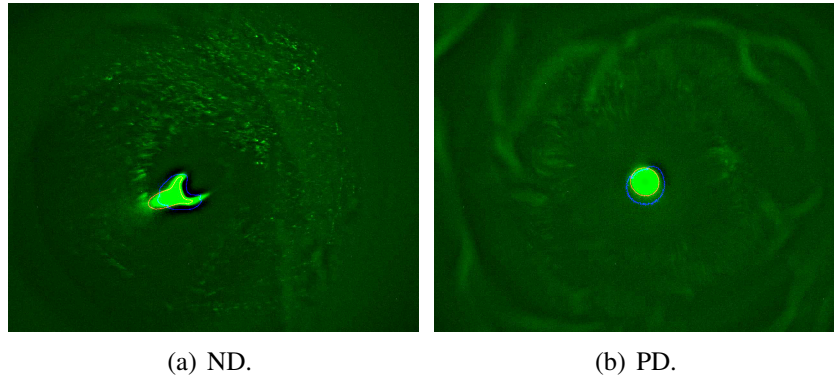


Figure 5.2 – Those images show the discrepancy in image information when the discharge polarity changes with the bigger magnification lens. The initial voltage was $2500V$ and the electrical current was $2mA$.

5.1 NEGATIVE DISCHARGE

The NDs were stable, meaning that the surface almost did not change in time. As already mentioned, the plasma was never straight down the nozzle, it was always displaced outwards. In a continuous discharge, the plasma had the same behaviour: it was steady and normally did not shift from the start point. The sequence in figure 5.3 shows these characteristics. Those figures were taken with $25SCCM$ of argon along with $-2000V$ and $2mA$, selected in the DC supply. The plasma is reaching the water surface in the left bottom sector of the pictures in figure 5.3.

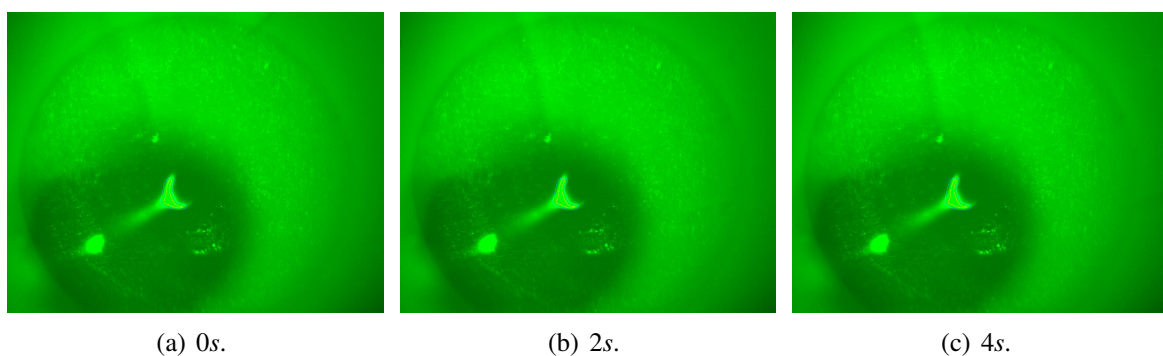


Figure 5.3 – Those images are separated by almost $2s$ and they are not changed.

In order to present the stability and continuity of the ND, the figure 5.4 shows the mean surface during $10s$ of plasma ignited. It also shows the surface height standard deviation. In the upper figure it is possible to affirm that the deepest point is where the discharge must

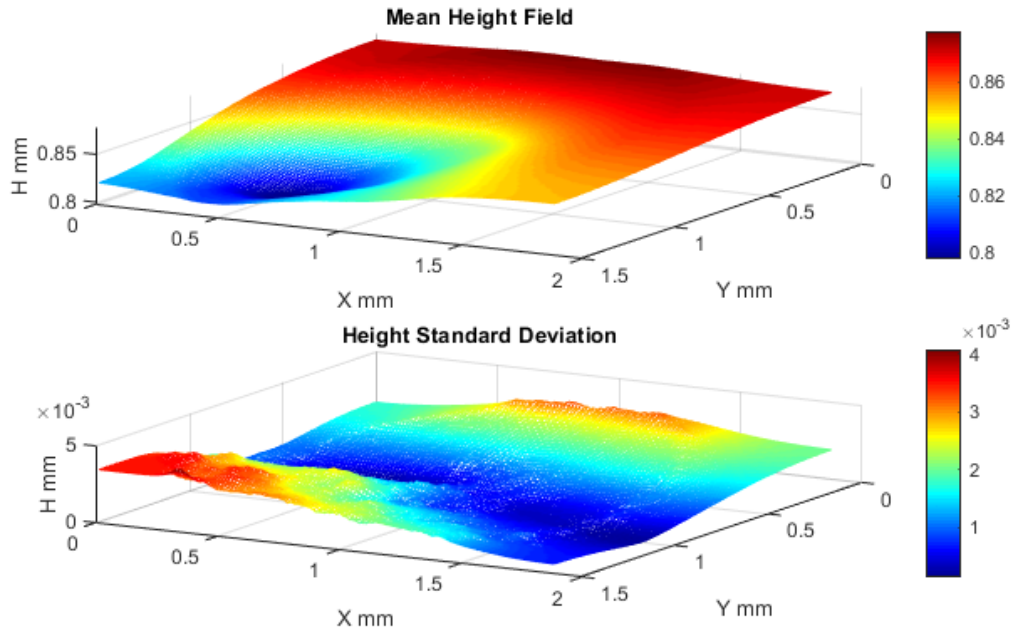


Figure 5.4 – Mean height and standard deviation for a $-2000V$, $2mA$ and $25SCCM$ plasma jet during 10s.

have touched the water surface. That point is closer to the highest deviation area and reveals that even the ND being continuous, close to the discharge contact, the surface has more movement.

For the continuation of the ND studies, discharges of various currents and also gas flow rates were seen. For current values, $1,5mA$, $3mA$ and $4,5mA$ were chosen. And in the gas side, flows of $5SCCM$, $10SCCM$, $15SCCM$ and $25SCCM$. The figure 5.5 shows the discharge nature for each pair, electrical current and argon flow rate.

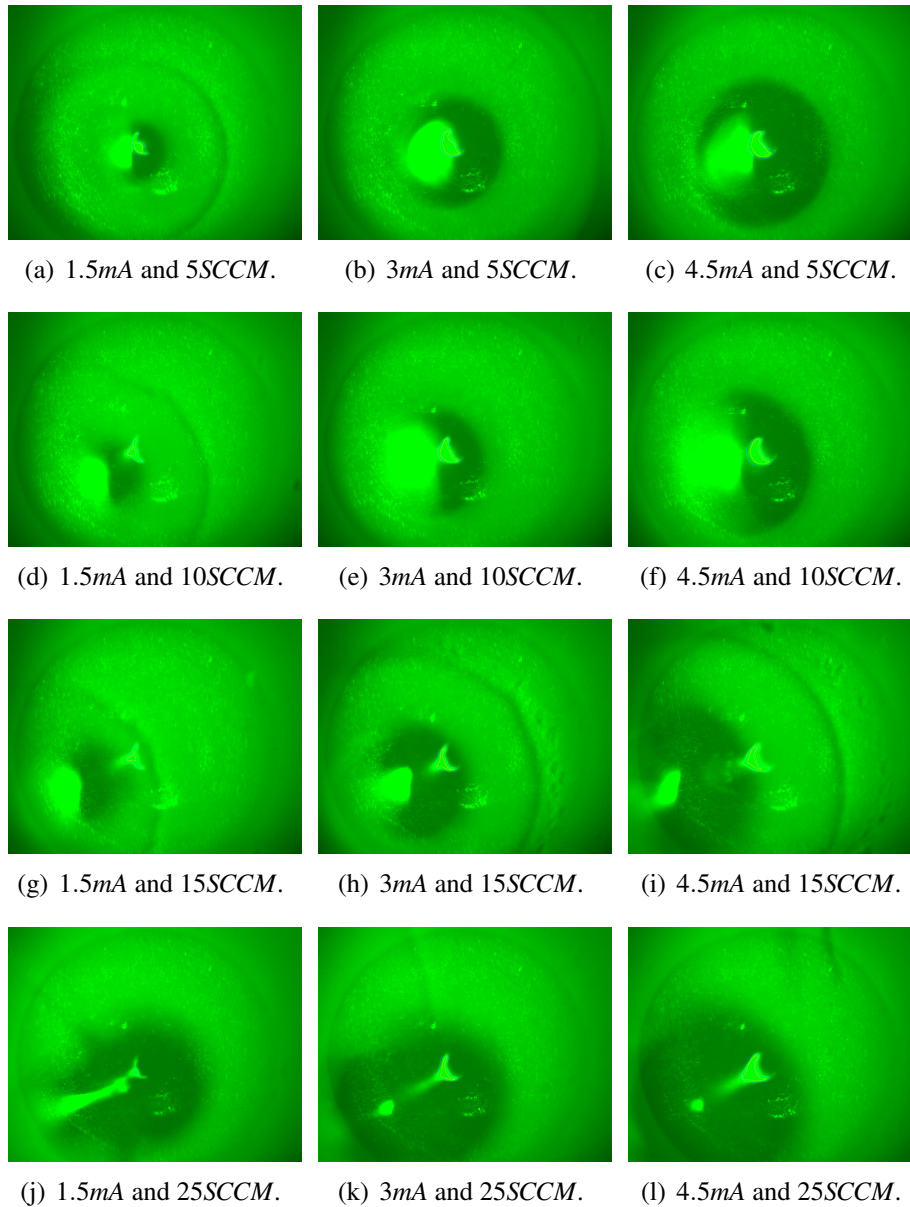


Figure 5.5 – Those images show, in columns, the gas flow differences and, in rows, the current differences.

5.1.1 ELECTRICAL CURRENT

For the electrical current differences, firstly, it is possible to observe a corona formation surrounding the discharge. That corona, seen in figure 5.5(a), was well defined and as the current raised this formation became bigger and went outside the field of vision. The second observation is that the main deformation in the middle was stronger as the current increased. A third observation is that the point of contact for the plasma stream was roughly at the same point regardless of the electrical current. However the size of the plasma has changed. A last

remark is the higher the gas flow, smaller was the current role in the surface deformation for those couples of current and flow rates.

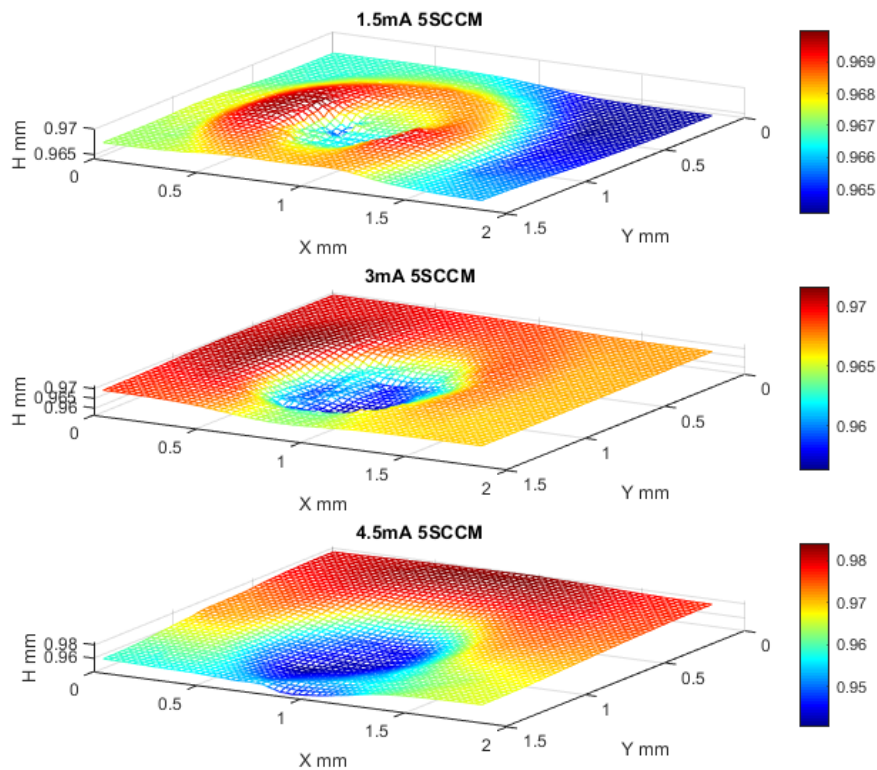


Figure 5.6 – Those images show the topography from figure 5.5(a),(b) and (c).

All the observable topography formations in figure 5.5 are represented in figure 5.6. The greater the current, wider the deformation. The central point of the depression is the darker part in figure 5.5. Another observable fact is that with 1,5mA and 5SCCM, the ND deformation was similar to when there was no plasma, showing a protuberance and a dimple.

5.1.1.1 CURRENT VARIATION FOR 5SCCM

When the current was varied, the surface had a different appearance but the most important point is that the depression was only wider and deeper. The main reason for that is probably the ionic wind that carries a fluid mass with the discharge. This phenomenon is caused by the negative ions that have a longer lifetime than positive ions. These ions carries the argon flow and accelerate it. The phenomenon is stable and keeps the argon in the water surface. It is explained in *Darny et al.*[12] for a helium plasma jet and it is called channelling

helium. Also, the ND is known for becoming spread in the receiver surface, water, so another possible point is that, probably with the increasing in current the contact area increases and so the deformation. According to *Y. Zhang, et al.*[11], the ND generates a wider velocity profile than the PD for a same tension, and *Darny et al.*[12] also explains that the negative ions are pushed radially from the discharge, so those explanations allied with a more powerful system could justify why there was a wider deformation as current was raised.

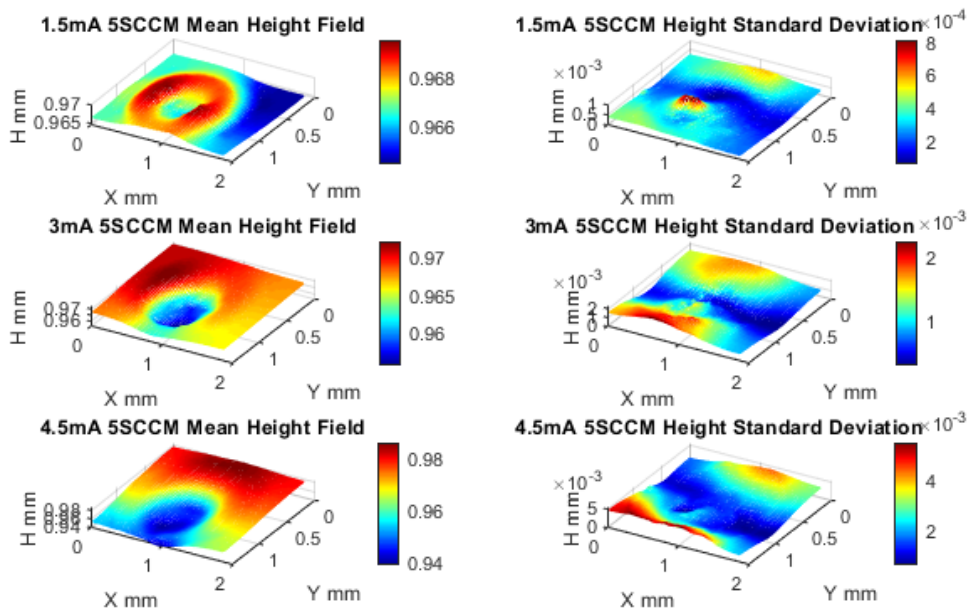


Figure 5.7 – Mean surface with its standard deviation for 1,5mA, 3mA and 4,5mA with 5SCCM of argon.

Remarks of the figure 5.7 are that the standard deviation were small and, for the smaller current, the biggest deviation was at the centre. For the other two, it changed to the left bottom corner closer to the mask limit.

5.1.1.2 CURRENT VARIATION FOR 10SCCM AND 15SCCM

The same behaviour occurred here, the only exception was for the first one where the "disc" disappeared and started to look like the other two. For 10SCCM and 15SCCM the fields had almost the same aspect. The mean field for 4,5mA in the 15SCCM flow rate is different from the 10SCCM and the probably explanation is in the gas flow rate variation

subsection 5.1.2. For simplification, the higher the current, stronger is the force diverting the flow pattern. However, the flow has seemingly an important role in the discharge pattern.

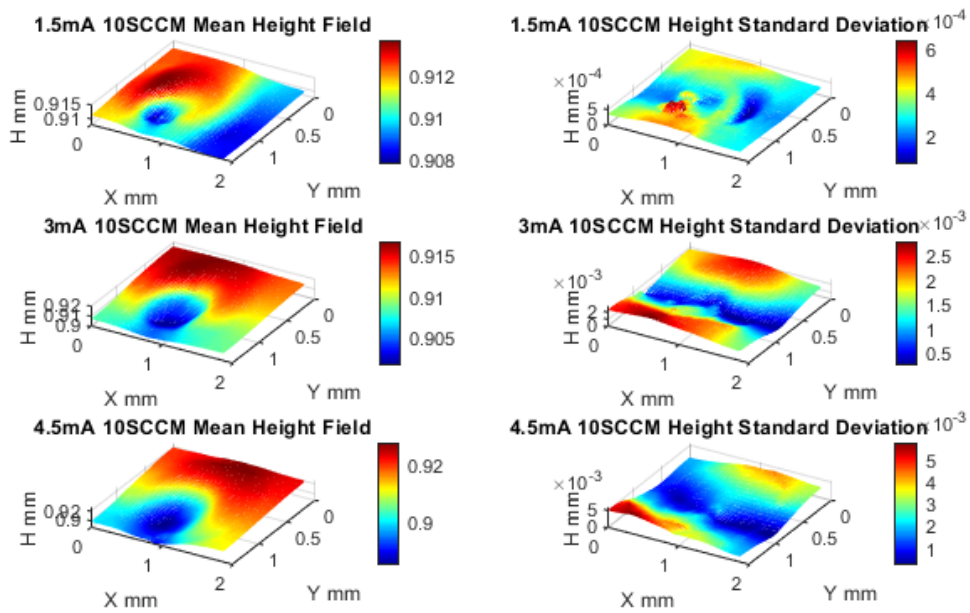


Figure 5.8 – Mean surface with its standard deviation for 1,5mA, 3mA and 4,5mA with 510CCM of argon.

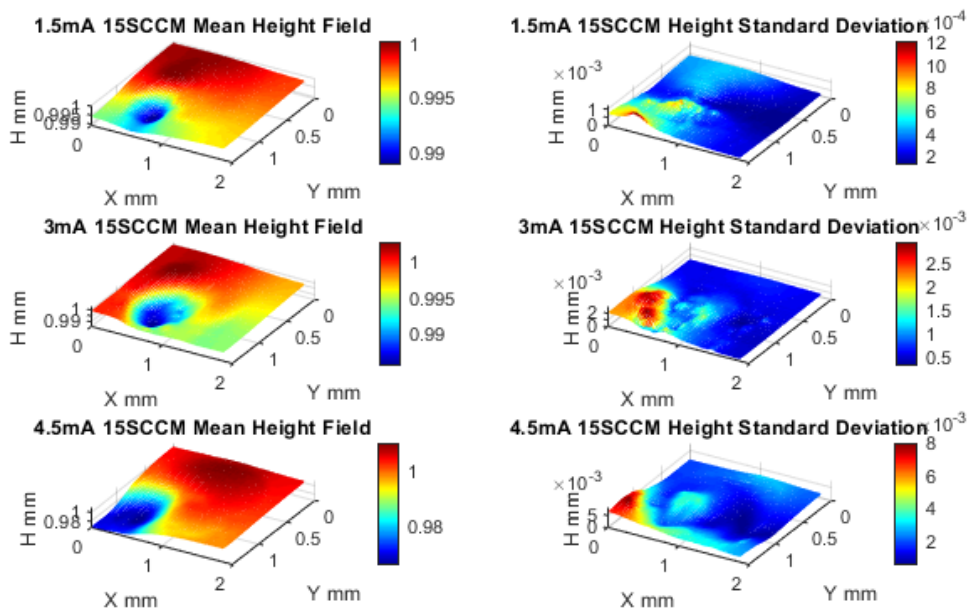


Figure 5.9 – Mean surface with its standard deviation for 1,5mA, 3mA and 4,5mA with 15SCCM of argon.

5.1.1.3 CURRENT VARIATION FOR 25SCCM

Here it is clearly that the current changes did not affected significantly the shape and size of the surface deformation. On the other hand, coupling high gas flow rate and high current, the discharge was diverted from the jet centre. A last observation in the standard deviation images is that, as the current increased, the deviation also increased and that could be seen as more action in the interface layer.

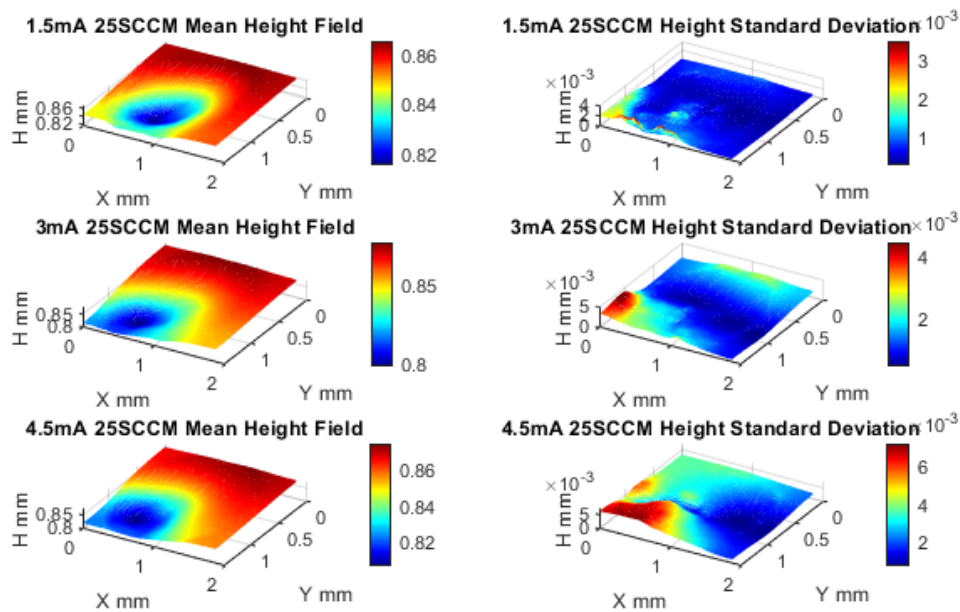


Figure 5.10 – Mean surface with its standard deviation for 1,5mA, 3mA and 4,5mA with 25SCCM of argon.

5.1.2 GAS FLOW RATES

For gas flow rates, the observations are that the contact point of the stream and the surface was dictated mostly by the gas. The second remark is that the corona reappeared when the gas flow was increased but also disappeared in the higher rate case, causing some sort of instability that maybe was not possible to be observed by this exposure time of the camera.

Moreover, as said in subsection 5.1.1.3 the current was not too important when the flow rate became higher. However, another observation could indicate that, as seen in figures 5.5(j),(k) and (l), the possible instability is maybe reduced by the rise in current, or it was

just a motion blur.

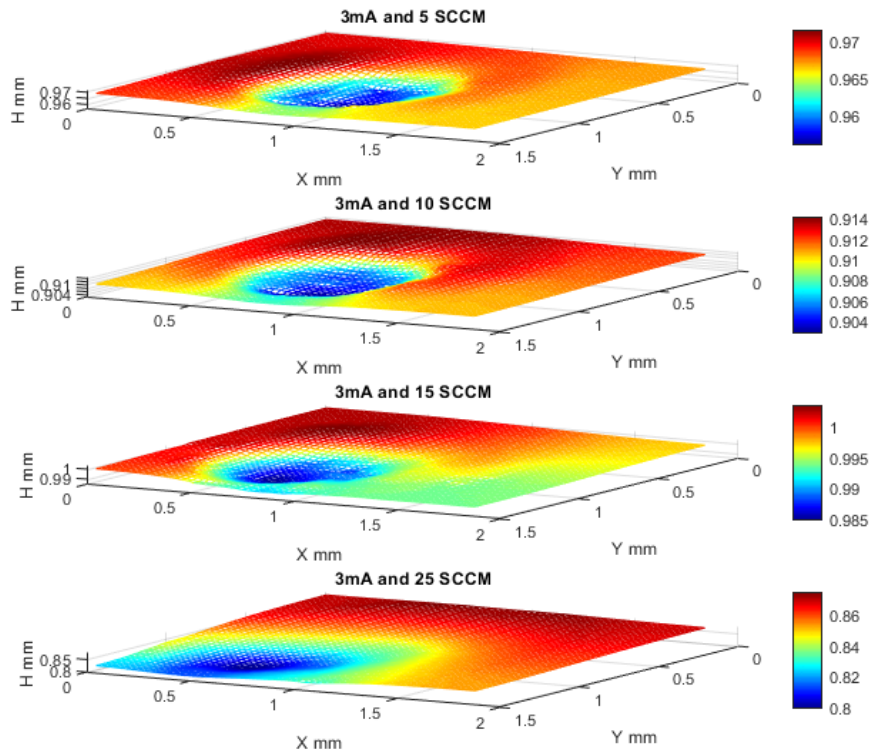


Figure 5.11 – Those images show the topography for 3mA and gas flow rates of 5SCCM, 10SCCM, 15SCCM and 25SCCM.

For the gas flow rates, the topography differences were smaller. The most perceptible thing in figure 5.11 is the variation in position of the depression. Another thing is that the deformation passed from a dimple and a flat surface to a spread region. As mentioned, the numerical values for the surface deformation must not be totally trusted, however here it is possible to see that with the rate growth the difference between the highest point to the lowest got bigger. The stronger deformation could be explained by the ionic wind also, where the a higher accelerate argon flow have more energy to be dissipated.

5.1.2.1 ARGON FLOW CHANGES FOR 1,5mA

In figure 5.12 the flow rate was changed from 5SCCM to 25SCCM and the current was kept at 1,5mA. The observable variation is that, when the flow rate increased, the deformation was shifted to the southwest side of the frame. However, when the flow was at 25SCCM

the deformation is stretched towards the centre of the jet.

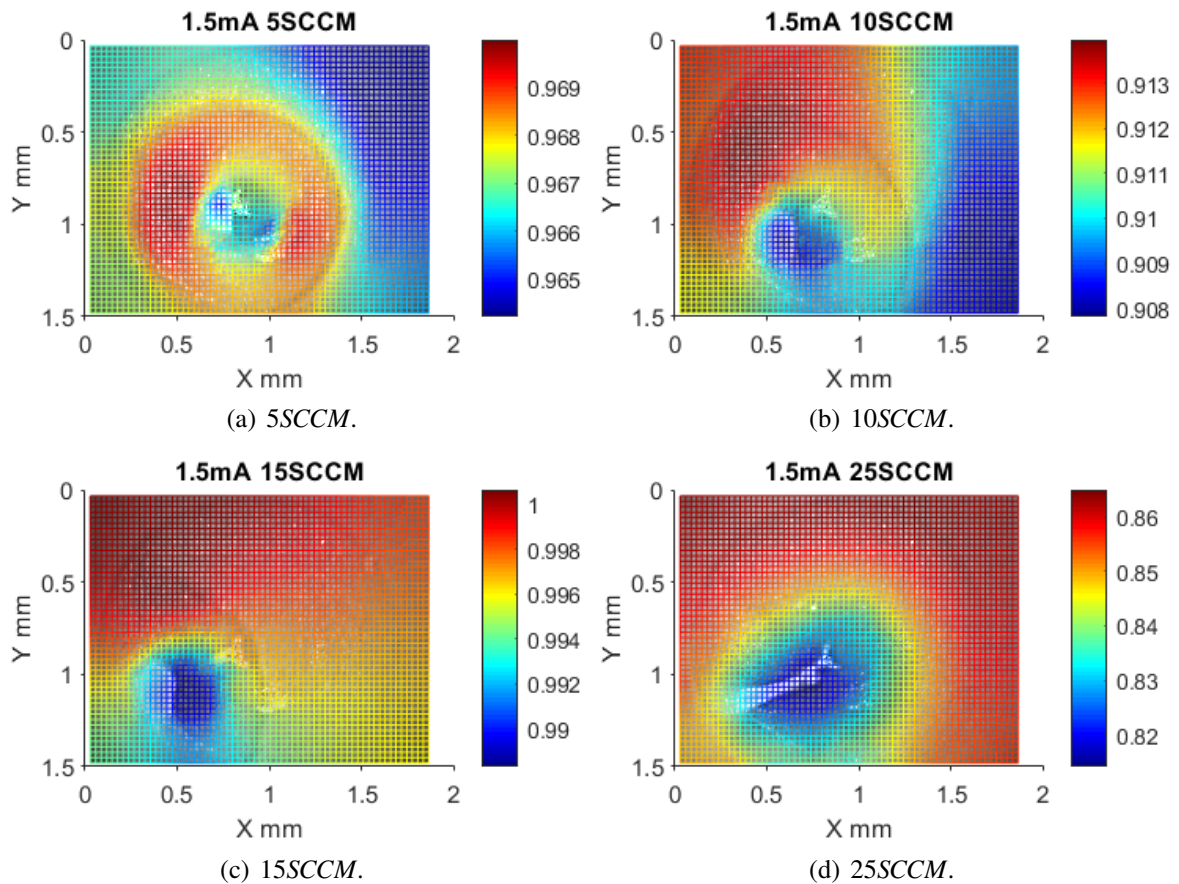


Figure 5.12 – Those images were composed by a electrical current of 1,5mA and the argon flow was changed.

Trying to explain the phenomenon it is possible to point out some physical reasons for the behaviour. Firstly, according to *Sosa et al.* [10], the electrohydrodynamic (EHD) force is determined by the current density, so an increase in current should provoke a greater EHD force. Thus, if there is something that makes the ND goes towards the lateral part, the path of the discharge will be not straight and a secondary flow is diverted to the lateral with the discharge, pulling the argon flow and the surroundings.

One assumption for the contact point to be placed in the outer part is that, maybe the height difference between the deepest point and the border is enough to promote the discharge to occur out of the centre. With 5SCCM the total deformation caused by the argon is small and the decrease in distance is insufficient to push the discharge far away from the centre. This aspect begins to be more pronounced as the flow increases.

But, the variation of the position while raising the flow rate could be possible because, as the flow increases, there is more argon molecules to be accelerated. Therefore, the deformation is possibly bigger and, as said, the discharge will be shifted making the plasma path carry the fluid around it. This phenomenon of generating EHD force is the momentum transfer from charged accelerated particles to neutral molecules by collision, according to *She Chen et al.* [9]. That is known as ionic wind and could possibly be the justification for this.

For the last one, figure 5.12(d), the stretched depression is probably because of a higher gas momentum due to its high velocity. With 25SCCM, the exit velocity in the nozzle is around 16m/s. Possibly due to the small distance from the water, the flow deviation is not totally achieved and it starts to deform the central region as well.

This behaviour is present in all three current cases seen in the followings parts.

5.1.2.2 ARGON FLOW CHANGES FOR 3mA

The same behaviour happened here, the initial discharge was closer to the centre, then it started to shift downwards and, finally, it was stretched. However, as the current was bigger, the deformation was also more defined, except for the 25SCCM. This was probably due to the high flow rate, although the inward part was smaller, if compared with the previous case. As said, an increase in current also increased the electric force deforming the flow pattern.

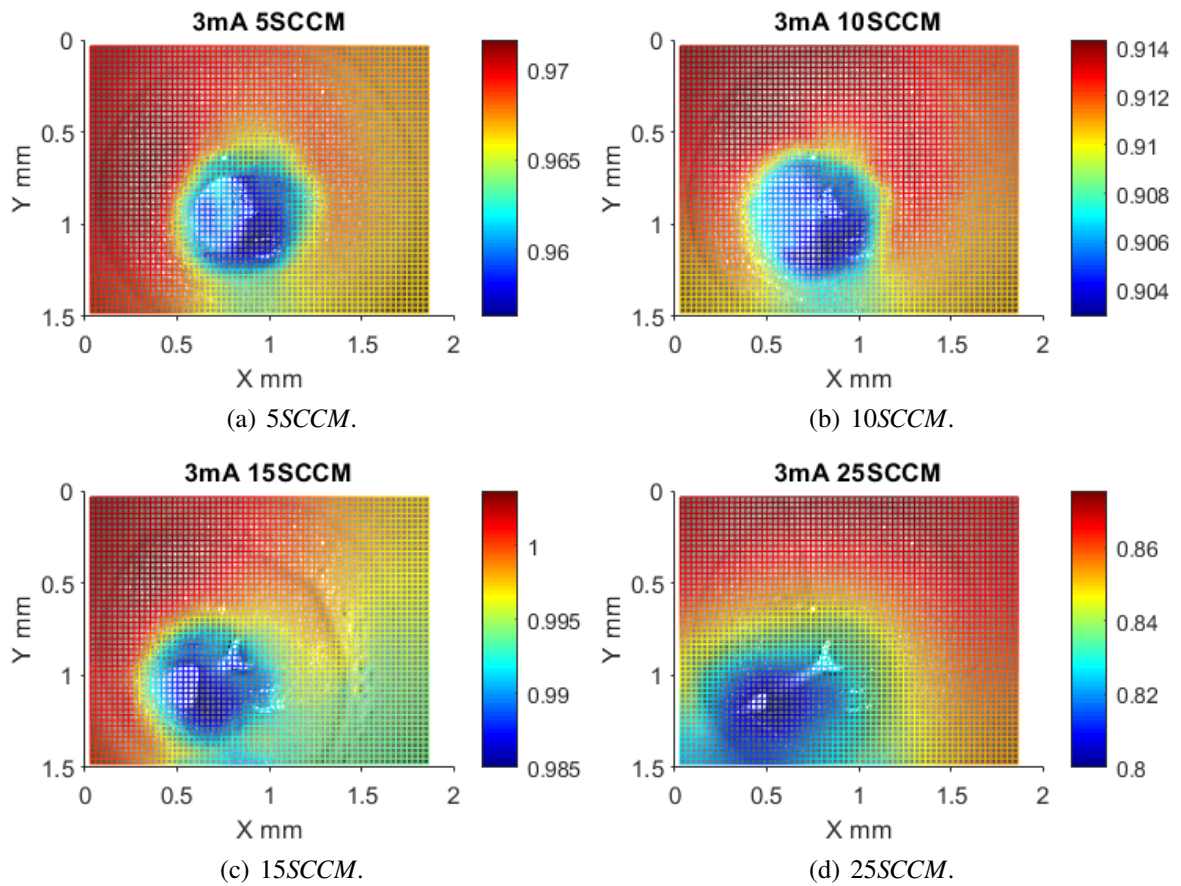


Figure 5.13 – Those images were composed by a electrical current of $3mA$ and the argon flow was changed.

5.1.2.3 ARGON FLOW CHANGES FOR 4,5mA

As always, the same process was present, however, possibly because of the highest current, the last combination of current and argon flow rate did not have the stretched portion. If compared to the bibliographic reference, *Kovačević et al.* [8] or *van Rens et al.* [7], their flow rates were much higher than the one used here. They worked in hundreds and thousands of *SCCM* and, at those flow rates, the gas has a bigger momentum and is not easily deviated.

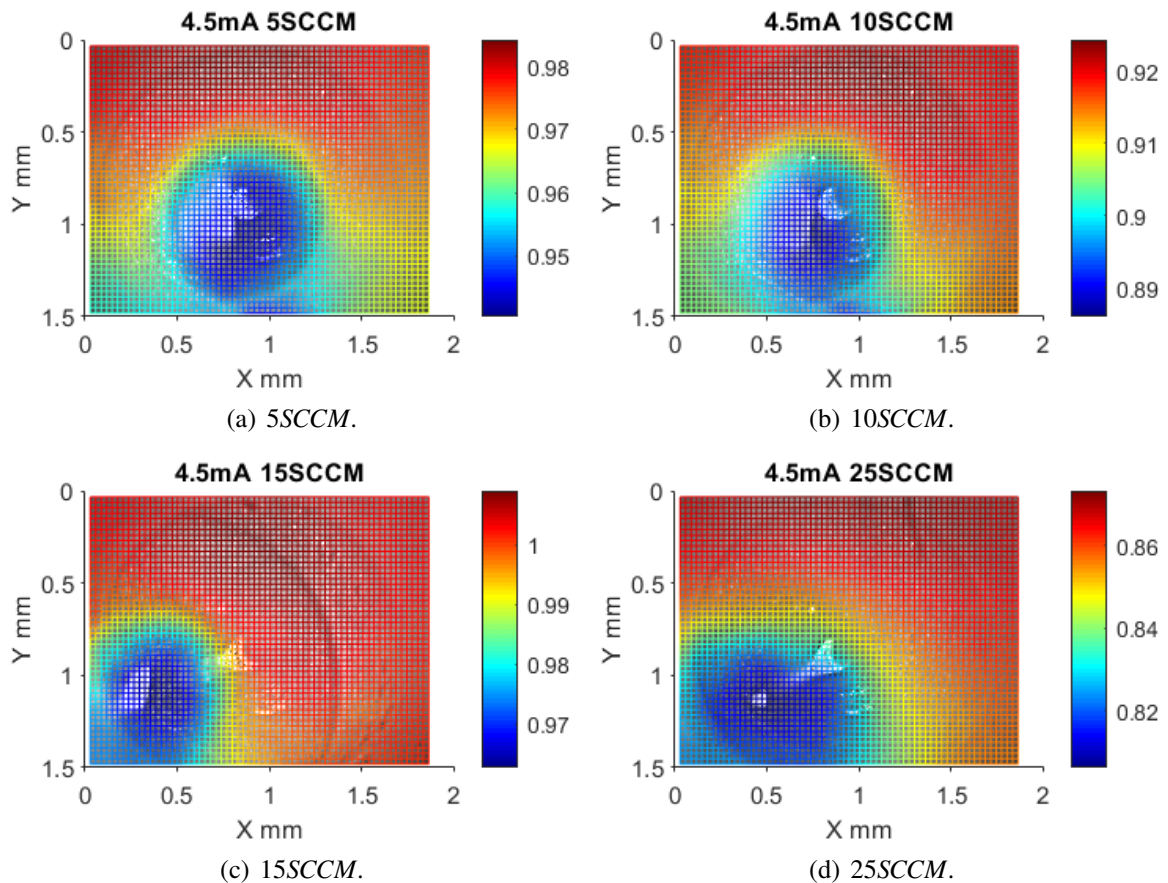


Figure 5.14 – Those images were composed by a electrical current of $4,5mA$ and the argon flow was changed.

5.2 POSITIVE DISCHARGE

For the PD, the process was different. The images were correlated but the results were not trusted for non of the series of images. As will be shown in next paragraphs and figures, the PD was a lot more energising and busier than the ND. It had a lot of fast deformations and changes that were impossible to observe with the actual FS-SS setup.

After all, even not correlated, it was possible to do some observations from the images. The first one is that the discharge point was right in the middle, vertically to the capillary tube. It was also continuous since it did not move around during the discharge. In figure 5.15 it is possible to see that there was a lot of movement in comparison with the ND already seen here. And, in the same figure, with a smaller exposure time, it is still not possible to clearly see the activity. Despite of that, the bright point in the middle was constant and

it corresponded to the discharge itself. According to *Darny et al.*[12], the PD generates downstream positive ions, that have short lifetimes, and also pulls negative ions, with longer lifetime and bigger masses. Those negative ions can have a destruction effect on the argon flow and that could be related to the disturbed behaviour of the PD.

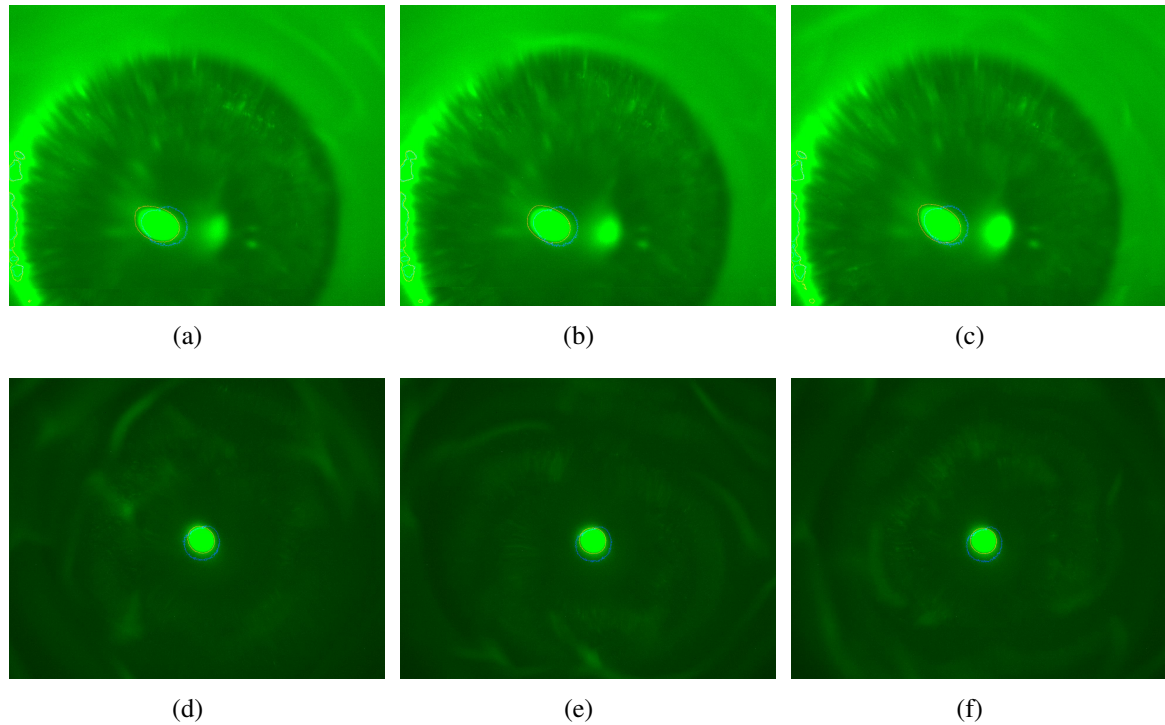


Figure 5.15 – PD for $3mA$. The first setup had a longer exposure time and the second one had a $5ms$ of exposure.

In order to obtain some information, a field of height calculation has been run, however, the results were not conclusive. The figure 5.16 shows the field of one step for both the faster and slower exposure times. For the fastest, figure 5.16(a), it is impossible to say anything about its topography, in contrast, for the second one, a mean effect generated by the longer exposure could show a smoother topography and even a dimple close to the discharge area.

For comparison, it is possible to see side by side the shadowgraph image from the ND and the PD, and see that, in PD, the liquid had a great amount of waves while in the negative there were fewer.

Another setup for FS-SS has been experimented, using the camera applied in shadowgraph. Even though it was clearer, the quality improvement was not sufficiently. With the new camera, an electrical current variation has been tried and has shown sufficient differ-

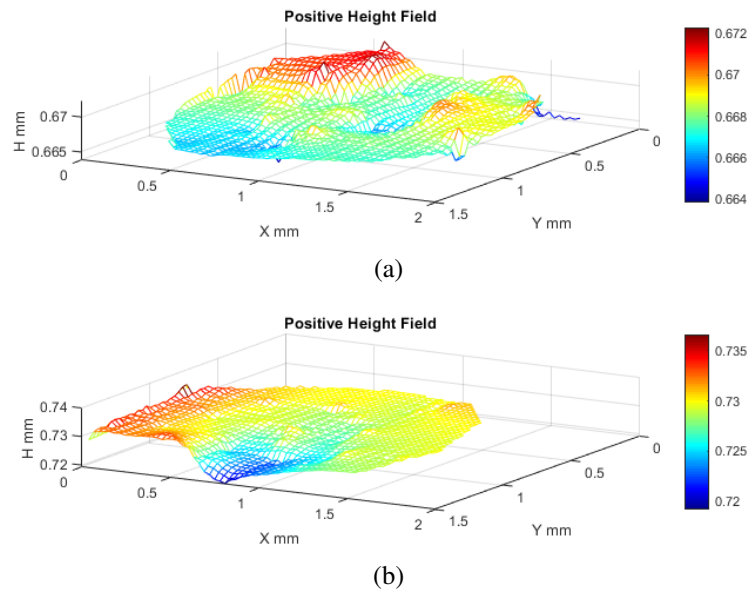


Figure 5.16 – The figure (a) is a surface for the fastest exposure and the figure (b) is for the longest exposure time. The second one has a mean effect, it even has the dimple in the middle.

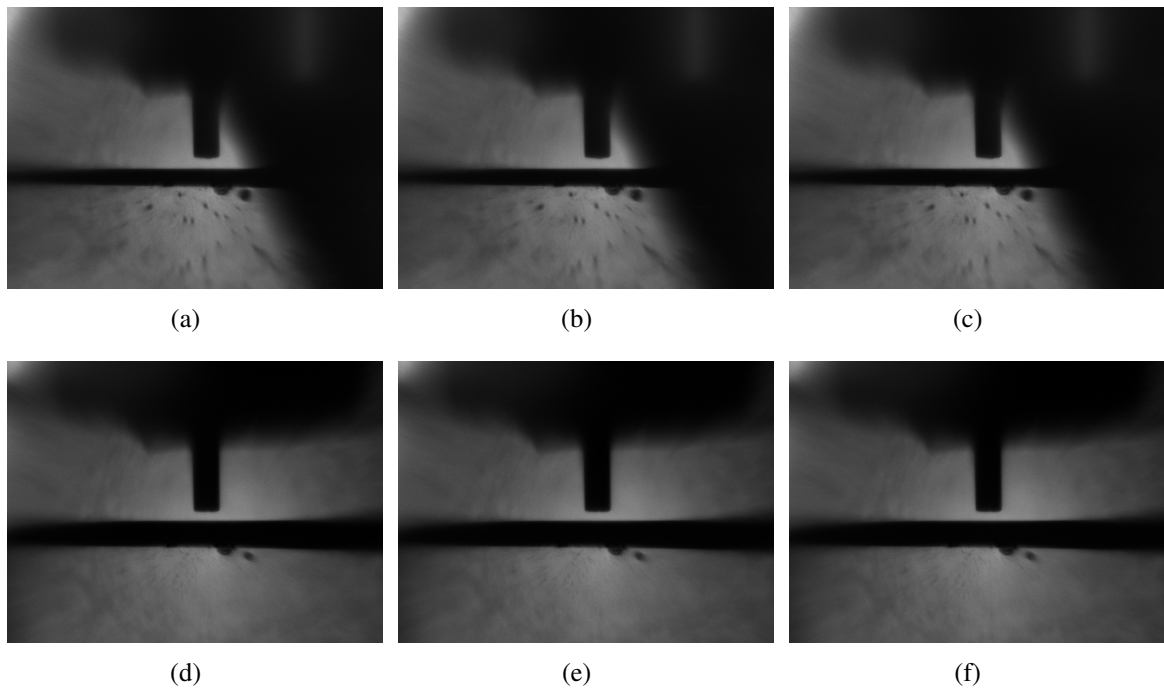


Figure 5.17 – The three in the top are from the PD and the others three are ND. It is not so clear to see the differences but when seen in sequence it comes up. However, it is possible to observe that the PD generated more bubbles in the liquid also.

ences. In figure 5.18, it is observable that it appears to have concentric waves getting out of the centre. Those waves in $1,8mA$ were sharpen and well defined, it is probably possible to obtain a wave formation frequency. When the current was raised, that good definition was

no longer present and it was substituted by more pinched, stretched and irregular lines. For the 4,5mA there was almost no longer a wave shape, it was closer to an instability or an unsteadiness. The last point is that, the white bright point that corresponds to the discharge, got bigger as the current was increased.

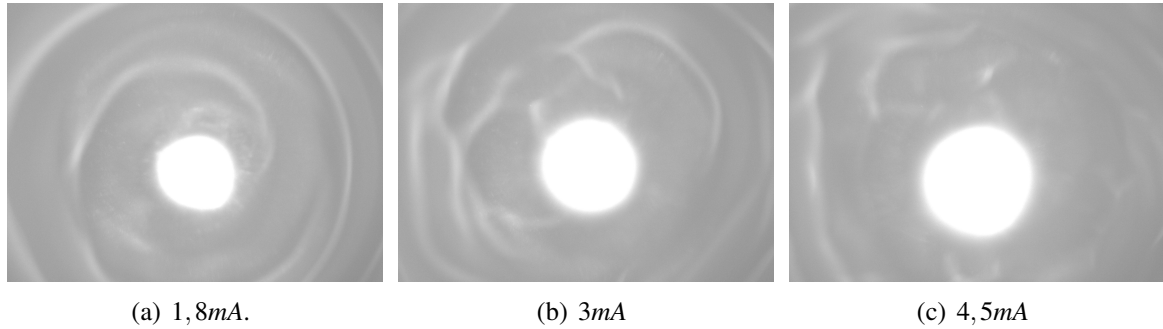


Figure 5.18 – Images from the other camera capable to see better formations in water surface.

6 CONCLUSION

The FS-SS method is a really powerful tool to work with, since it is capable of many tasks and, even though, the setup need to be more illuminated, the method has shown good results. For the magnified pictures, the lightened area was smaller and consequently brighter, so that privileged the smaller lens, though it has a small field of view. The ideal combination would be a brighter source of light with the greater lens, less zoom. In addition, for the PD, the possible problem is the long exposure time and for that, a brighter light can make the camera see clearly in a smaller time, but it also depends in the camera speed. With the same LED controlled by the same equipment, the camera needs to be more sensible. A ideal solution could be to illuminate the pattern and the nozzle by another system, separated from the camera line, such as a background illumination as used in *Moisy et al.* [3]. This configuration does not require a beam splitter in the camera line, which doubles the brightness of the image already.

Concerning the optical and plasma jet systems, the ideal configuration to have a big field of view is to place the pattern and the nozzle at the same plane. By doing that, almost no mask would be needed. But for that, the pattern and the support need to interfere as minimum

as possible in the electric field. If the pattern interferes too much with the system, the result deformation could not be compared with an application without the pattern. Furthermore, with the pattern in that position, it is difficult to ignite and stabilise the plasma. It would be preferable to have an option that is less intrusive.

As for the discharges, the improvement in knowledge about the surface topography is a great advance. Primarily, the inside region and the outside air have already been studied, but the surface was not studied yet. Now, after those results, some behaviours and characteristics are known and could be useful for future researches.

For the ND, the deformation area with the biggest changes are close to the contact point. In the flow rate range, the deformation changes within current and flow velocity. Also, the mean surface has a dimple as seen in *van Rens et al.* [7] independently in the gas flow and current configurations. For the next steps, a more physical approach to the problem is envisaged and maybe a study focused in the discharge contact point.

For the PD, the conclusions are different. Overall, the surface topography was not achieved because of the difficulties in correlation. A faster camera and a brighter light source could allow a better visualisation and, consequently, a topography result. However, as already seen, the PD has more movement than the ND. So maybe it would be useful to try a more statistical approach than an instantaneous one. An idea is to link the electrical signal with the image seen in figure 5.18, in order to correlate the peaks and valleys in the signal to a possible corresponding wave in the figure.

References

- [1] Bittencourt, J.A. Fundamentals of plasma physics 1 J.A. Bittencourt.-3rd ed. p. cm. Includes index. ISBN 978-1-4419-1930-4 ISBN 978-1-4757-4030-1 (eBook)
DOI : 10.1007/978 – 1 – 4757 – 4030 – 1
- [2] Thomas Orriere et al. Effect of plasma polarity on the synthesis of graphene quantum dots by atmospheric-pressure microplasmas. 2020 *Nanotechnology* 31 485001.
DOI : 10.1088/1361 – 6528/abaa11
- [3] Moisy F, Rabaud M & Salsac K. A synthetic Schlieren method for the measurement of the topography of a liquid interface. *Exp Fluids* 46, 1021 (2009).
DOI : <https://doi.org/10.1007/s00348-008-0608-z>
- [4] P J Bruggeman et al. Plasma–liquid interactions: a review and roadmap. 2016 *Plasma Sources Sci. Technol.* 25 053002.
DOI : 10.1088/0022 – 3727/46/27/275201
- [5] J T Holgate et al 2019 *New J. Phys.* 21 063002 Simulated dynamics of a plasma-sheath-liquid interface.
DOI : 10.1088/0963 – 0252/25/5/053002
- [6] W Van Gaens and A Bogaerts, 2013 *J. Phys. D: Appl. Phys.* 46 275201 Kinetic modelling for an atmospheric pressure argon plasma jet in humid air.
DOI : 10.1088/0963 – 0252/25/5/053002
- [7] J. F. M. van Rens, J. T. Schoof, F. C. Ummelen, D. C. van Vugt, P. J. Bruggeman and E. M. van Veldhuizen, "Induced Liquid Phase Flow by RF Ar Cold Atmospheric Pressure Plasma Jet," in *IEEE Transactions on Plasma Science*, vol. 42, no. 10, pp. 2622-2623, Oct. 2014.
DOI : 10.1109/TPS.2014.2328793
- [8] Vesna V Kovačević et al., 2018 *J. Phys. D: Appl. Phys.* 51 065202 The effect of liquid target on a nonthermal plasma jet—imaging, electric fields, visualization of gas flow and

optical emission spectroscopy.

DOI : 10.1088/1361 – 6463/aaa288

- [9] She Chen, R G W van den Berg and S Nijdam, Published 30 May 2018 • © 2018 IOP Publishing Ltd, The effect of DC voltage polarity on ionic wind in ambient air for cooling purposes.

DOI : [https://doi.org/10.1088/1361 – 6595/aabd5f](https://doi.org/10.1088/1361-6595/aabd5f)

- [10] Sosa R, Artana G, Grondona D, Kelly H, Márquez a and Minotti F, J. Phys. D. Appl. Phys. 40 663–73, 2007, Discharge characteristics of plasma sheet actuators.

- [11] Yu Zhang, Lijuan Liu, Yang Chen, Jiting Ouyang, Journal of Electrostatics, Volume 74, 2015, Pages 15-20, ISSN 0304-3886, Characteristics of ionic wind in needle-to-ring corona discharge.

DOI : <https://doi.org/10.1016/j.elstat.2014.12.008>

- [12] T Darny, J-M Pouvesle, J Fontane, L Joly, S Dozias and E Robert, Published 13 September 2017 • © 2017 IOP Publishing Ltd, Plasma Sources Science and Technology, Volume 26, Number 10, Plasma action on helium flow in cold atmospheric pressure plasma jet experiments.

DOI : [https://doi.org/10.1088/1361 – 6595/aa8877](https://doi.org/10.1088/1361-6595/aa8877)

- [13] Wildeman, S. Real-time quantitative Schlieren imaging by fast Fourier demodulation of a checkered backdrop. Exp Fluids 59, 97 (2018).

DOI : [https://doi.org/10.1007/s00348 – 018 – 2553 – 9](https://doi.org/10.1007/s00348-018-2553-9)

- [14] Thielicke, W., Sonntag, R. (2021) Particle Image Velocimetry for MATLAB: Accuracy and enhanced algorithms in PIVlab. Journal of Open Research Software, 9: 12.

DOI : <https://doi.org/10.5334/jors.334>

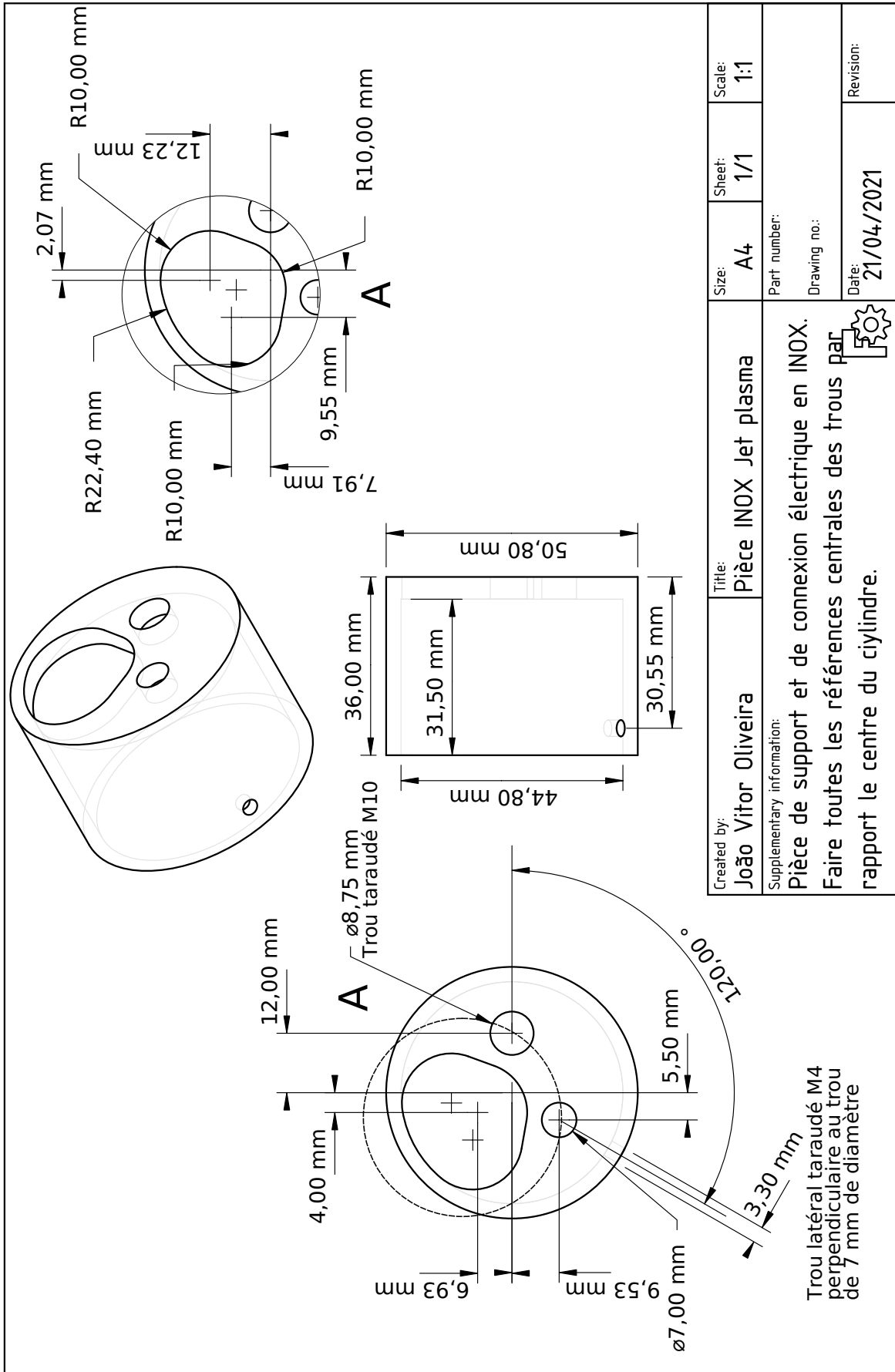
- [15] Thielicke, W. and Stamhuis, E.J. (2014): PIVlab – Towards User-friendly, Affordable and Accurate Digital Particle Image Velocimetry in MATLAB. Journal of Open Research Software 2(1):e30.

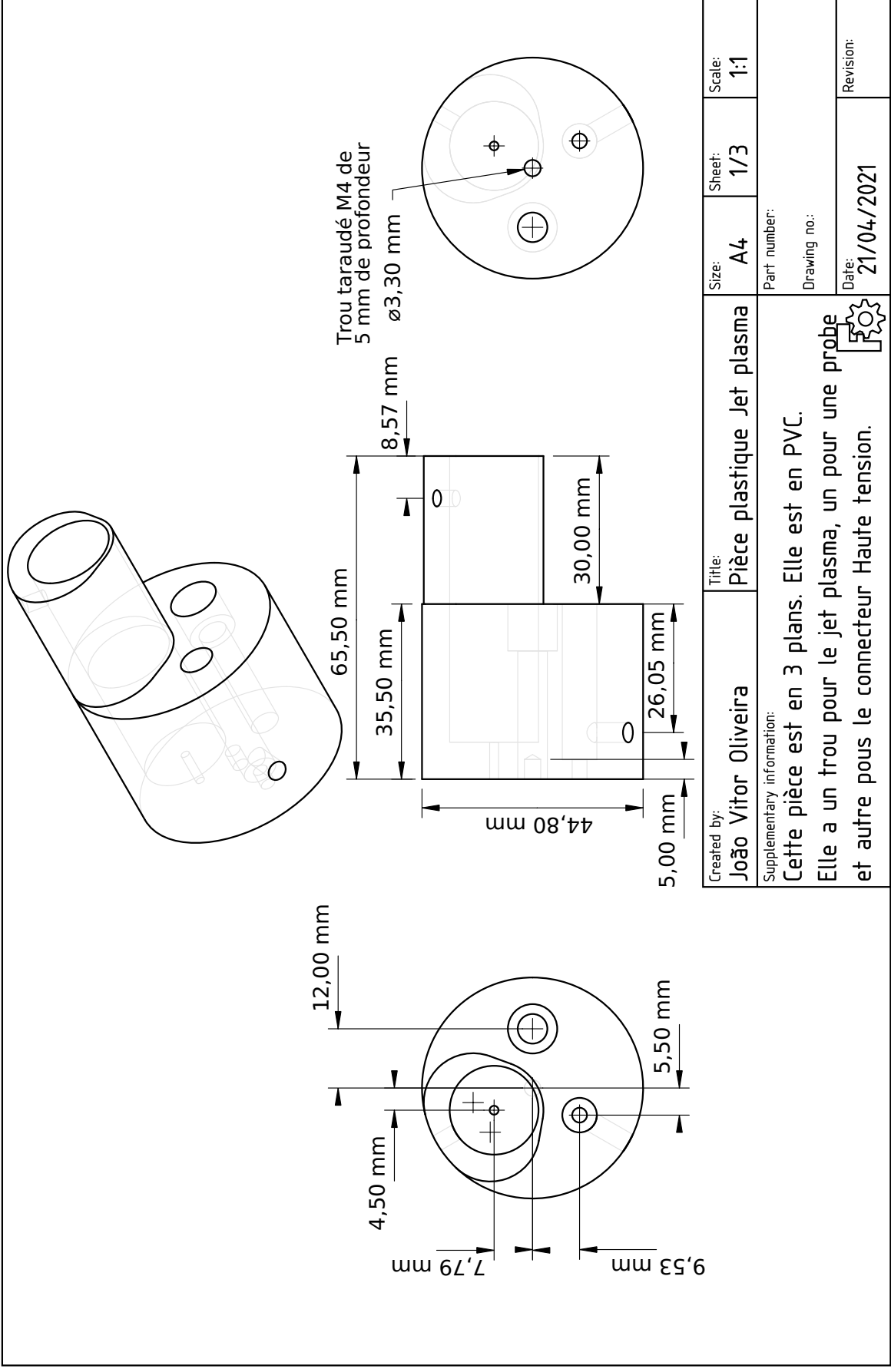
DOI : <http://dx.doi.org/10.5334/jors.bl>

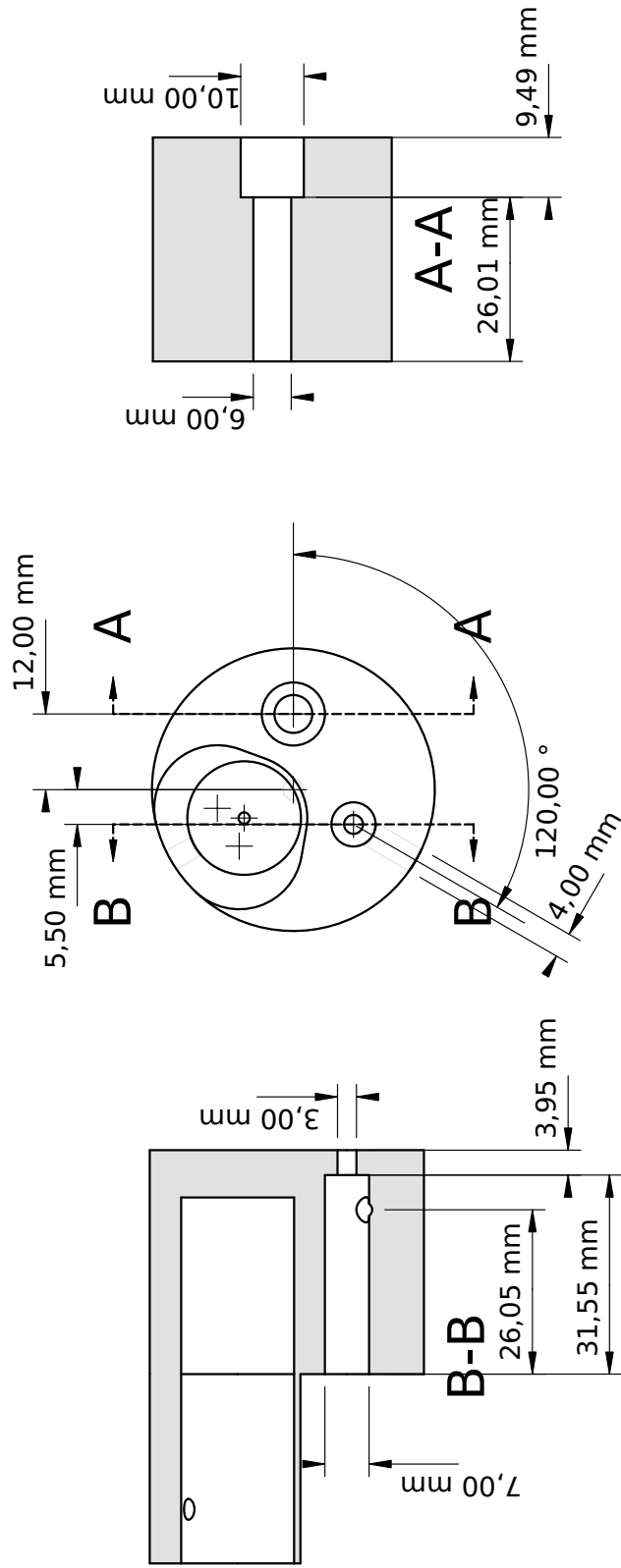
[16] Thielicke, W. (2014): The Flapping Flight of Birds - Analysis and Application. Phd thesis, Rijksuniversiteit Groningen.

DOI : [http : //irs.ub.rug.nl/ppn/382783069](http://irs.ub.rug.nl/ppn/382783069)

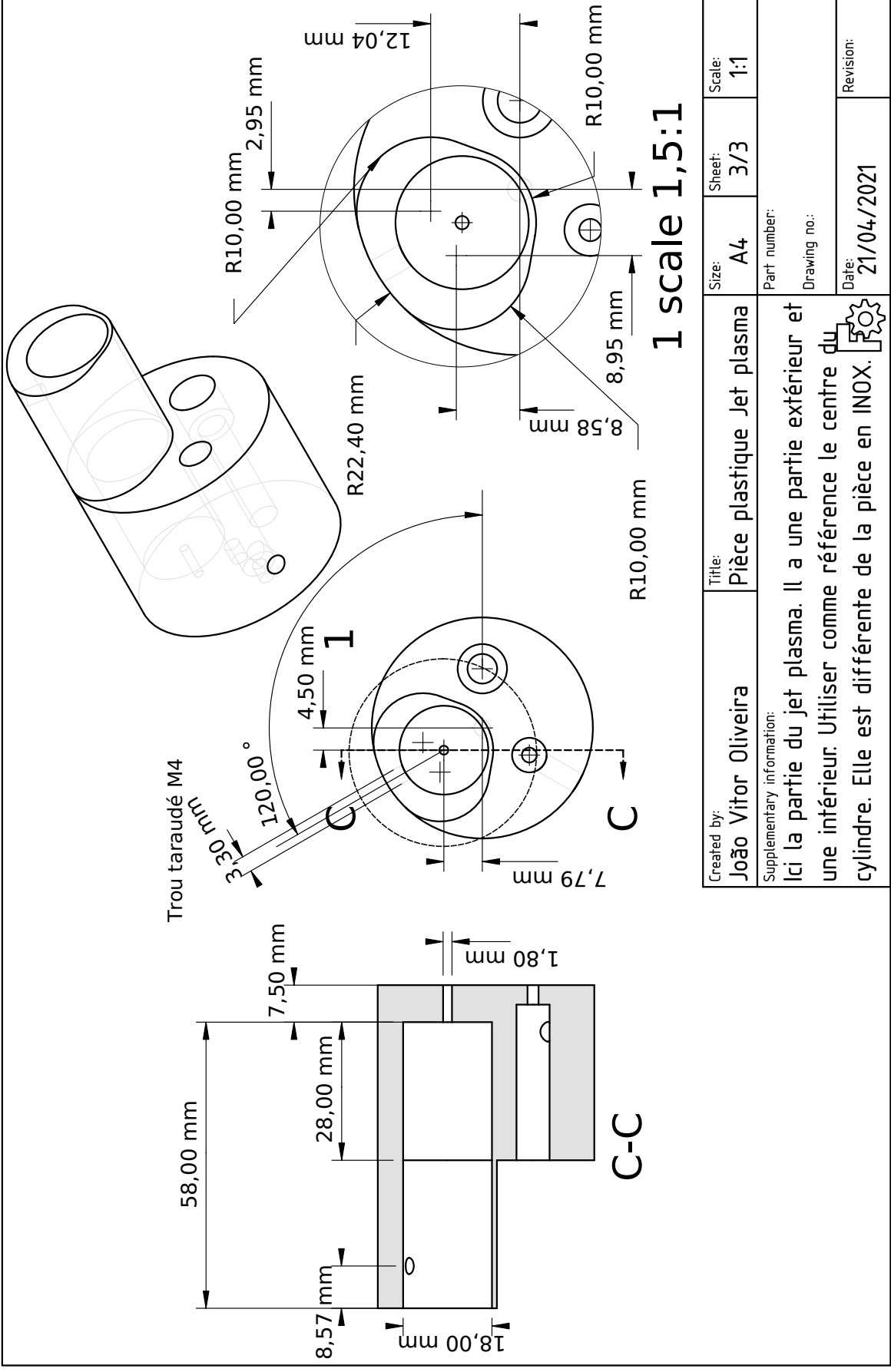
7 APPENDIX

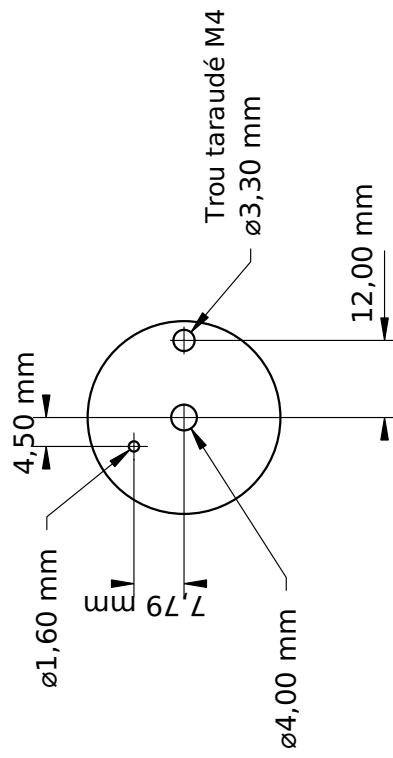
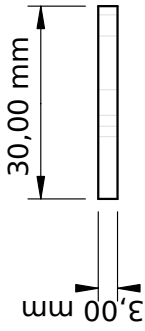






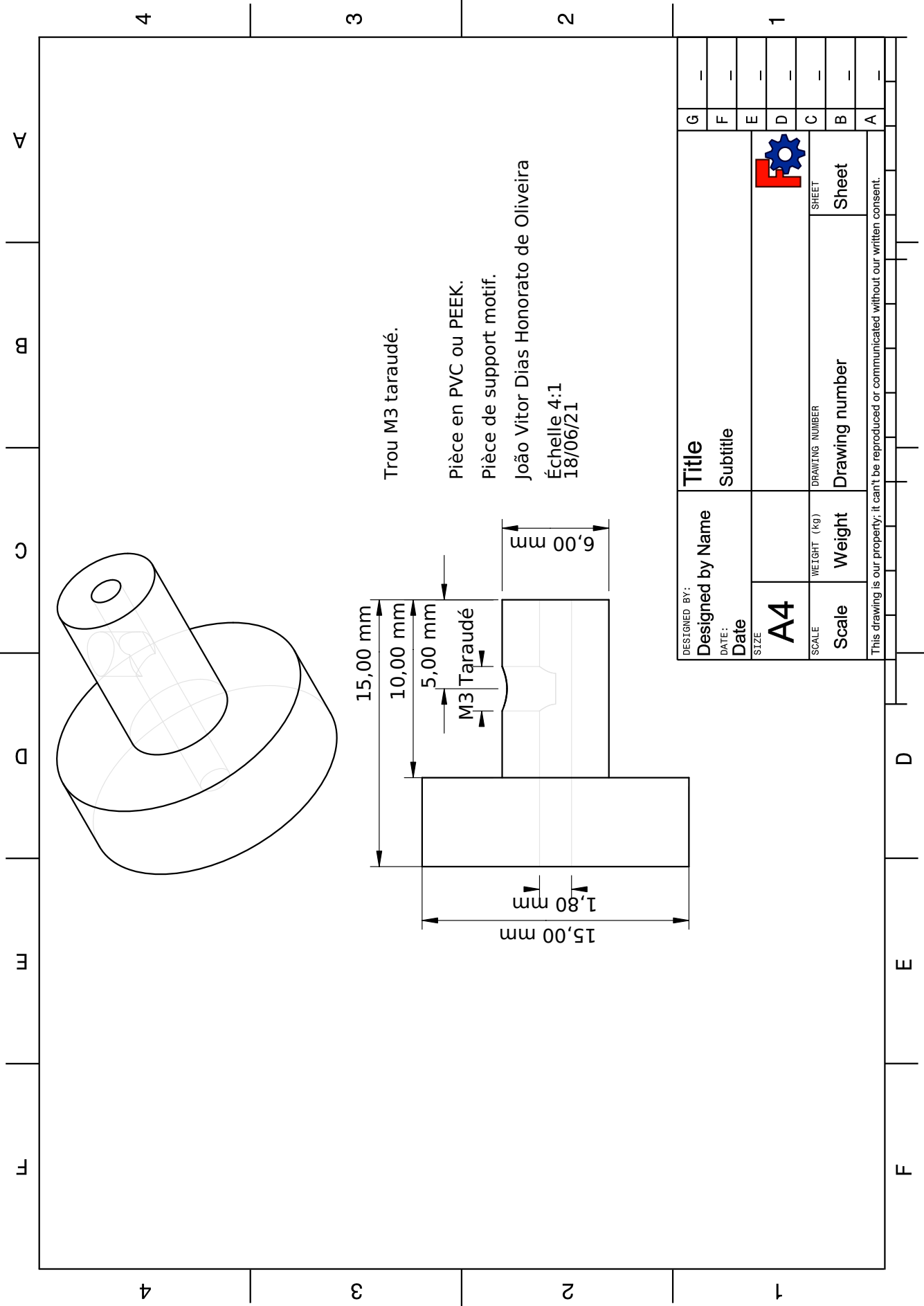
Created by: João Vitor Oliveira	Title: Pièce plastique Jet plasma	Size: A4	Sheet: 2/3	Scale: 1:1
Supplementary information: Ici on voit les vues en coupe du connecteur, A-A, et de la probe, G-C. On peut voir aussi le trou lateral de 4mm et qui va jusqu'au trou de la probe.		Part number:		Revision:
		Drawing no.:		Date: 21/04/2021
				Revision:





Created by: João Vitor Oliveira	Title: <Pièce> Jet plasma	Size: A4	Sheet: 1/1	Scale: 1:1
Supplementary information: Pièce en INOX pour lier les trois parties du support vissée par le centre.		Part number: Drawing no.:		Revision:
			Date: 21/04/2021	Revision:





Trou M3 taraudé.

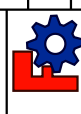
Pièce en PVC ou PEEK.

Pièce de support motif.

João Vitor Dias Honorato de Oliveira

Échelle 4:1

18/06/21

DESIGNED BY:		Title		G	
Designed by Name		Subtitle		F	
DATE:				E	
Date				D	
SIZE		A4		C	
SCALE		WEIGHT (kg)		SHEET	
Scale		Drawing number		Sheet	
This drawing is our property; it can't be reproduced or communicated without our written consent.					
				A	